Title

Antifungal action of the combination of ferulic acid and ultraviolet-A irradiation against *Saccharomyces cerevisiae*

Author names

A. Shirai [1,2], H. Kunimi [3] and K. Tsuchiya [4]

Affiliations

[1] Department of Bioscience and Bioindustry, Graduate School of Technology, Industrial and Social Sciences, Tokushima University, 2-1 Minami-Josanjima, Tokushima 770-8513, Japan.

[2] Institute of Post-LED Photonics, Tokushima University, 2-1 Minami-Josanjima, Tokushima 770-8506, Japan.

[3] Graduate School of Advanced Technology and Science, Tokushima University, 2-1 Minami-Josanjima, Tokushima 770-8506, Japan.

[4] Department of Medical Pharmacology, Institute of Biomedical Sciences, Graduate School of Tokushima University, 1-78-1, Sho-machi, Tokushima 770-8505, Japan.

Running headline: Photoantifungal action of ferulic acid

Corresponding author: Akihiro Shirai

Department of Bioscience and Bioindustry, Graduate School of Technology, Industrial and Social Sciences, Tokushima University, 2-1 Minami-Josanjima, Tokushima 770-8506, Japan.

e-mail: a.shirai@tokushima-u.ac.jp

Co-authors

Haruka Kunimi, e-mail: laboratory.notebook923@gmail.com

Present affiliation: NICHIA CORPORATION, Anan-shi, Tokushima, Japan.

Koichiro Tsuchiya, e-mail: tsuchiya@tokushima-u.ac.jp

Keywords: antifungal action, ferulic acid, ultraviolet-A, synergism, oxidative stress, pyruvate kinase 1

Abstract (within 300 words)

Aims

To examine the antifungal action of photocombination treatment with ferulic acid (FA) and ultraviolet-A (UV-A) light (wavelength, 365 nm) by investigating associated changes in cellular functions of *Saccharomyces cerevisiae*.

Methods and Results

When pre-incubation of yeast cells with FA was extended from 0.5 to 10 min, its photofungicidal activity increased. Flow cytometry analysis of stained live and dead cells revealed that 10-min UV-A exposure combined with FA (1 mg ml^{-1}) induced a ~ 99.9% decrease in cell viability although maintaining cell membrane integrity when compared with pre-exposure samples. When morphological and biochemical analysis were performed, treated

cells exhibited an intact cell surface and oxidative DNA damage similar to control cells. Photocombination treatment induced cellular proteins oxidation, as shown by 2.3-fold increasing in immunostaining levels of ~49-kDa carbonylated proteins compared with pre-irradiation samples. Pyruvate kinase 1 (PK1) was identified by proteomics analysis as a candidate protein whose levels was affected by photocombination treatment. Moreover, intracellular ATP levels decreased following FA treatment both in darkness and with UV-A irradiation, thus suggesting a possible FA-induced delay in cell growth.

Conclusions

FA functions within the cytoplasmic membrane; addition of UV-A exposure induces increased oxidative modifications of cytosolic proteins such as PK1, which functions in ATP generation, without causing detectable genotoxicity, thus triggering inactivation of yeast cells.

Significance and Impact of Study

Microbial contamination is a serious problem that diminishes the quality of fruits and vegetables. Combining light exposure with food-grade phenolic acids such as FA is a promising disinfection technology for applications in agriculture and food processing. However, the mode of photofungicidal action of FA with UV-A light remains unclear. This study is the first to elucidate the mechanism using *S. cerevisiae*. Moreover, proteomics analyses identified a specific cytosolic protein, PK1, which is oxidatively modified by photocombination treatment.

55

56 **Introduction**

57 Ferulic acid (FA) is an abundant phytochemical phenolic acid present in plants such as
58 bamboo shoots, red cabbage, oranges, rice, and wheat (Kumar and Pruthi 2014). Research
59 indicates that FA forms ester and amide cross-links with a wide variety of natural products. FA
60 form ester cross-links with polysaccharides and cell wall lignin (Rosazza *et al*. 1995). FA also
61 exhibits potential therapeutic antioxidant, hepatoprotective, cholesterol-lowering, and
62 anti-inflammatory activities (Paiva *et al*. 2013). In addition, FA has antimicrobial activity,
63 although it is relatively weak, with reported minimum inhibitory concentrations of ≥1 mg ml^{-1}
64 for bacteria and fungi (yeasts and filamentous fungi) (Zabka and Pavela 2013; Shirai *et al*.
65 2017).

66 Studies have shown that the antimicrobial activity of FA increases markedly when used in
67 combination with ultraviolet-A (UV-A) light (315-400 nm) irradiation. Many reports have
68 described similar bactericidal synergism of naturally occurring phenolic acids such as coumaric
69 acid, caffeic acid (CaA), and gallic acid when combined with UV-A light irradiation at
70 wavelengths from 365 to 400 nm (Nakamura *et al*. 2012; Nakamura *et al*. 2015; Cossu *et al*.
71 2016; Nakamura *et al*. 2017; Shirai *et al*. 2017; de Oliveira *et al*. 2021). Such photodynamic
72 antimicrobial chemotherapy (PACT) approaches combine non-toxic photosensitizers with

73 irradiation in the light-emitting wavelength range appropriate for photoexcitation reactions.
74 Reactive oxygen species (ROS), including H_2O_2 and hydroxyl radical, are involved in the
75 synergistic antimicrobial activity of phenolic acids. Chemical assays using colorimetric methods
76 and electron spin resonance have confirmed the generation of ROS after exposure of phenolic
77 acid solutions to UV-A irradiation. These ROS are responsible for the photobactericidal activity,
78 as evidenced by reductions in activity in the presence of ROS quenchers (Nakamura *et al*. 2012;
79 Shirai *et al*. 2015). PACT using natural compounds that differ from synthetic organic
80 compounds in conjunction with light fits the 'clean green technology concept' and is a
81 potentially promising approach for effectively killing pathogenic and spoilage microorganisms
82 in the fields of agriculture and food processing.

83 Applications of the polyphenolic compound curcumin (diferuloyl methane; a non-toxic
84 natural dye extracted from plants), whose structure closely resembles an FA dimer, have been
85 extensively studied. The antimicrobial activity is enhanced under visible light (400-500 nm)
86 irradiation and affects a number of microorganisms, including various bacteria and fungi
87 (Dovigo *et al*. 2011; Jiang *et al*. 2014; Temba *et al*. 2016). The mechanism of action reportedly
88 involves disruption of the cell wall, cytoplasmic membrane, and mitochondrial membrane
89 potential, in addition to nuclear fragmentation and defects in the ergosterol biosynthesis
90 pathway, induced by increased curcumin-mediated intracellular ROS accumulation (Jiang *et al*.

91 2014; Kumar *et al*. 2014; Wei *et al*. 2021).

92 de Oliveira *et al*. (2021) conducted screening assays for bactericidal synergism of
93 treatments combining phenolic acids with UV-A light irradiation of *Escherichia coli* O157:H7.
94 Only a few studies examining the mode of photoantimicrobial action of phenolic acids,
95 including FA, have been reported (Nakamura *et al*. 2012; Nakamura *et al*. 2015; Nakamura *et al*.
96 2017; Shirai and Yasutomo 2019). We previously demonstrated that the photobactericidal
97 mechanism of UV-A light in the presence of FA involves increased oxidative modifications and
98 subsequent disruption of the bacterial membrane in *E. coli* without detectable genotoxicity
99 (Shirai and Yasutomo 2019). In contrast, data regarding the synergistic fungicidal activity of
100 phenolic acids elicited by light exposure remain poor.

101 Mycotoxin-producing fungi that contaminate food can cause serious human mycoses and
102 therefore represent a serious problem in the food industry (Bernardi *et al.* 2018). Food-spoilage
103 yeasts such as the genera *Saccharomyces* and *Zygosaccharomyces* are primarily responsible for
104 the deterioration of fresh and stored fruits and vegetables and of products made from fruits and
105 vegetables by causing softening, formation of off-flavors and off-odors, and undesirable ethanol
106 fermentation (Krisch *et al.* 2016). Although the photoantifungal efficiency of FA has been
107 investigated against four fungi, including *S. cerevisiae* (Shirai *et al*. 2017), the mode of
108 photofungicidal action of phenolic acids such as FA remains unclear.

109 The objective of the present research was to elucidate the mechanism of FA-mediated
110 fungicidal activity under UV-A light irradiation of *S. cerevisiae* as an experimental fungus of the
111 genus *Saccharomyces* by investigating associated changes in cellular functions. The results of
112 this study could aid in the development of a clean, green disinfection technology combining
113 UV-A light irradiation with food-grade phenolic acids such as FA for applications to eliminate
114 microbial contaminants in agriculture and food processing.
115
116 **Materials and Methods**
117
118 **Chemicals**
119 FA was purchased from the Tokyo Chemical Industry Co., Ltd. (Tokyo, Japan). An FA stock
120 solution was prepared at 100-fold of the assay concentration, 100 mg ml^{-1}, by dissolving the
121 compound in 80% dimethylsulfoxide (DMSO). ε-Polylysine solution (EPL; 25%) was obtained
122 from JNC Corporation (Tokyo, Japan). All other experimental materials were purchased from
123 commercial sources.
124
125 **Light source and irradiation**
126 All antifungal activity experiments were performed using a device equipped with a UV-A

127 LED (NCSU033B; Nichia Corp., Anan, Japan), which emits in the range 360 to 370 nm, with a
128 365-nm peak wavelength, as described previously (Shirai *et al*. 2014). The irradiance was
129 adjusted to 4.77 mW cm^{-2} by changing the distance of the sample from the LED and measured
130 according to a previous method (Shirai *et al*. 2017). All assays were performed at 30 °C in an
131 incubator box using a suspension of yeast cells in plastic Petri dishes (90 mm × 15 mm,
132 Ecopetri ELS; Sansyo Co., Ltd., Tokyo, Japan). The yeast sample dish was placed on a magnetic
133 stirrer (to provide continuous mixing), and 4 LEDs were positioned over the dish; the total
134 irradiance was 19 mW cm^{-2}, based on an irradiance of 4.77 mW cm^{-2} per LED.
135
136 **Photofungicidal assay**
137 All assays were performed with *S. cerevisiae* NITE Biological Resource Center (NBRC)
138 1136. The culture conditions were as described previously (Shirai *et al*. 2017). Yeast
139 suspensions were prepared after incubation in Sabouraud broth for 24 h at 28 °C, and cell
140 densities were determined by monitoring the optical density at 660 nm. Yeast suspensions were
141 prepared in sterile ion-exchanged water at a prescribed cell density (2-3 × 10^5 or × 10^7 colony
142 forming units [CFU] ml^{-1}) and then transferred to plastic petri dishes. A stock solution of FA was
143 added to the yeast suspension by 100-fold dilution to 1 mg ml^{-1} before initiating UV-A
144 irradiation. Fungicidal activity against strain NBRC 1136 was determined by counting the CFU

145 according to a previous report (Shirai *et al*. 2017). Colony counts were determined using
146 Sabouraud agar plates (Nissui Pharmaceutical Co. Ltd., Tokyo, Japan) after incubation for 72 h
147 at 28 °C. For samples exposed to UV-A irradiation alone (without FA) and control samples
148 (absence of both FA and irradiation), DMSO was added to a final concentration of 0.8% instead
149 of FA.
150

151 **Photofungicidal assay against yeast cells pre-incubated with FA**

152 Photofungicidal activity following FA pretreatment was investigated using a modification of
153 a previously published method (Shirai and Yasutomo 2019). A 5-min light exposure was
154 performed after the yeast suspensions (2-3×10^5 CFU ml^{-1}) including FA (1 mg ml^{-1}) were
155 incubated for 0.5, 2, 5, or 10 min with stirring. Yeast viability was then measured as described
156 above.
157

158 **Staining assay for flow cytometry**

159 Changes in membrane permeability were assessed using Cyto 9 and propidium iodide (PI)
160 staining (Live/Dead Fungalight Yeast Viability and Counting kit; Thermo Fisher Scientific Inc.,
161 Waltham, MA, USA) according to a previously described method with some modifications
162 (Berney *et al*. 2006). Yeast cell suspensions (2-3 × 10^7 CFU ml^{-1}) were treated with FA at 1 mg

163 ml^{-1} and irradiated for 5 and 10 min. An aliquot (1 ml) of each sample was then centrifuged to

164 pellet the yeast cells (6500*g*, 3 min, 20 °C), and the resulting cell pellet was washed twice with

165 Dulbecco's phosphate-buffered saline (D-PBS[−], abbreviated hereafter as PBS; Nacalai Tesque,

166 Inc., Kyoto, Japan) and then resuspended in PBS. After dual staining with Cyto 9 and PI at 1 μl

167 ml^{-1} each for 15 min at 37 °C, the stained cells were analyzed using a FACS Verse (Becton

168 Dickinson, Franklin Lakes, NJ, USA) flow cytometer. Simultaneously, fungal viability after

169 each treatment was assayed as described above. Assay samples included cells treated with UV-A

170 alone, FA alone, and EPL (100 mg l^{-1}), and the samples were also analyzed after staining

171 according to the method described above.

172 The proportion of damaged or dead cells (permeable to PI) was expressed as the percentage

173 per 10,000 cells counted. The number of viable cells was determined using the colony counting

174 method described above.

175

176 **Scanning electron microscopy (SEM)**

177 Suspensions of yeast cells (2-3 × 10^7 CFU ml^{-1}) were treated with FA (1 mg ml^{-1}), UV-A

178 irradiation, a combination of the two, or EPL (100 mg l^{-1}). All treatments lasted 10 min.

179 Processing of the treated cells and SEM observation using a S-4700 (Hitachi Ltd., Tokyo, Japan)

180 were performed as described previously (Shirai *et al*. 2009).

181

182 **Measurement of DNA oxidation**

183 An aliquot (1 ml) of yeast cells treated as described in the section "Staining assay for flow
184 cytometry" was washed twice with PBS and centrifuged to obtain a cell pellet. Cell lysis and
185 DNA purification were carried out using a NucleoSpin Microbial DNA kit (Takara Bio Inc.,
186 Shiga, Japan) according to the manufacturer's protocol. Oxidation of purified DNA (9 μg 150
187 μl^{-1}) was quantified using a competitive enzyme-linked immunosorbent assay kit (Highly
188 Sensitive 8-OHdG Check; Japan Institute for the Control of Aging, Nikken SEIL Corp.,
189 Shizuoka, Japan) as described previously (Shirai *et al*. 2014).

190

191 **Immunodetection of carbonylated proteins**

192 Yeast cells treated with a combination of FA (1 mg ml^{-1}) and UV-A light exposure (3 and 10
193 min) were collected as described in the section "Staining assay for flow cytometry" and lysed
194 using Y-PER Yeast Protein Extraction Reagent (Thermo Fisher Scientific Inc.). The lysate was
195 centrifuged (12,000*g*, 10 min, 20 °C), and the concentration of protein in the supernatant was
196 measured using a Pierce BCA Protein Assay kit (Thermo Fisher Scientific Inc.). The sample was
197 then adjusted to a protein concentration of 824 μg ml^{-1} in 6% SDS solution and denatured.

198 Carbonylated proteins were immunodetected using an OxyBlot Protein Oxidation Detection

199 kit (Merck KGaA, Darmstadt, Germany) according to a previously described method (Qin *et al*.
200 2011) and the manufacturer's protocol. Carbonylated protein in the denatured protein sample (5
201 μg) was derivatized to 2,4-dinitrophenylhydrazone (DNP). The modified proteins (5 μg 20 μl^{-1})
202 were separated by 12% SDS-PAGE (Mini-protean TGX Gels; Bio-Rad Laboratories, Inc., Irvine,
203 CA, USA) and transferred onto a PVDF membrane (Immobilon-P; Merck KGaA) using a
204 blotting system (WSE-4020; ATTO Corp., Tokyo, Japan). Modified proteins were detected
205 using anti-DNP antibodies and visualized using a chemiluminescence detection kit (Immobilon
206 Western Chemiluminescent HRP Substrate, Merck KGaA). The luminescence intensity of each
207 band was recorded using a LuminoGraph (WSE-6100H-CS; ATTO Corp.).
208

209 **In-gel digestion, mass spectrometry, and database searching**

210 In-gel digestion was carried out according to a previously described method with some
211 modifications (Qin *et al*. 2011). Following combined treatment of yeast cells with FA (1 mg
212 ml^{-1}) and UV-A exposure, the protein solution was prepared in the same manner described
213 above. Protein samples prepared to a protein concentration of 12 μg μl^{-1} after reaction with
214 SDS-PAGE sample buffer (Sample Buffer Solution with Reducing Reagent [6×] for
215 SDS-PAGE; Nacalai Tesque, Inc.) for 5 min at 95 °C were separated by 12% SDS PAGE
216 (Mini-protean TGX Gels; Bio-Rad Laboratories, Inc.). To monitor sample loading, Coomassie

217 Brilliant Blue (CBB) R-250 (Quick-CBB; FUJIFILM Wako Pure Chemical Corp.) was used to
218 stain the proteins in the SDS gel. A protein band of approximately 50.8 kDa was observed and
219 manually excised from the gel and destained with 25 mmol l^{-1} NH_4HCO_3 in 50% (v/v)
220 acetonitrile (AN) solution for 10 min, and this procedure was repeated until destaining was
221 sufficient. The gel piece was dehydrated in AN, completely dried in a vacuum centrifuge
222 (MV-100; TOMY SEIKO Co., Ltd., Tokyo, Japan), and treated with reducing agent (10 mmol l^{-1}
223 dithiothreitol in 25 mmol l^{-1} NH_4HCO_3) prior to subsequent treatment with alkylating agent (55
224 mmol l^{-1} iodoacetamide in 25 mmol l^{-1} NH_4HCO_3). After washing twice with 25 mmol l^{-1}
225 NH_4HCO_3, the gel piece was immersed in 25 mmol l^{-1} NH_4HCO_3 in 50% (v/v) AN, and the
226 solution was replaced with 100% AN. After the sample was completely dried in a vacuum
227 centrifuge, enzymatic digestion was performed by addition of 30 μl of trypsin solution (20 ng
228 μl^{-1} in 25 mmol l^{-1} NH_4HCO_3). The digestion reaction was carried out overnight at 37 °C, after
229 which the excess trypsin solution was removed, and 25 mmol l^{-1} NH_4HCO_3 was added. Digested
230 peptides were extracted by three changes of 0.1% trifluoroacetic acid in 50% AN and
231 concentrated to a volume of approximately 25 μl using a vacuum centrifuge. After desalting
232 using a ZipTip C18 (Merck KGaA), the solution was subjected to MALDI-TOF mass
233 spectrometry analysis (Autoflex speed-TK; Bruker Japan K.K., Kanagawa, Japan).
234 For database searching, the generated peak lists were uploaded to the MASCOT Peptide

235 Mass Fingerprint program on the Matrix Science (London, U.K.) public website
236 (http://www.matrixscience.com) and searched against SwissProt databases with a taxonomy
237 restriction of '*Saccharomyces cerevisiae* (baker's yeast)'. Trypsin was selected as the proteolytic
238 enzyme, and one missed cleavage was permitted. Carbamidomethylation (C) of cysteine was
239 selected as a fixed modification. The peptide mass tolerance, mass of the charge carrier, and
240 mass value were set to ±150 ppm, MH^+, and monoisotopic, respectively.
241
242 **Intracellular ATP content measurement and growth curve determination**
243 Following a 2-min pre-incubation of yeast cells (approximately 2-3×10^5 CFU ml^{-1}) after
244 addition of FA (1 mg ml^{-1}), cells were irradiated with UV-A light for 3 min. The intracellular
245 ATP content was determined using a Luciferin/luciferase kit (Lucifell AT100; Kikkoman
246 Biochemifa Company, Chiba, Japan) according to the manufacturer's protocol. Intracellular ATP
247 was extracted using an ATP-releasing reagent in a 10-s reaction after decomposition of
248 extracellular ATP using an ATP-eliminating reagent in a 30-min reaction. Simultaneously,
249 samples treated with FA alone (without light), with light exposure alone, and with neither FA
250 nor light (as a control) for 3 min were also analyzed as described above. These samples were
251 also pre-incubated for 2 min before treatment under each condition. Cell viability was
252 determined by counting CFU.

253 An aliquot (0.05 ml) of a suspension of yeast cells treated under each of the above
254 conditions was mixed with 0.05 ml of sterile water followed by 0.1 ml of Sabouraud liquid
255 broth prepared at a 2-fold concentration containing 0.005% (w/v) Tween 80 (FUJIFILM Wako
256 Pure Chemical Corp.) in a 96-well culture plate (Corning Inc., New York, NY, USA). The
257 culture plate was subsequently sealed with sealing tape (Thermo Fisher Scientific Inc.). Yeast
258 growth in each well was monitored at an optical density at 650 nm (OD_{650}) every 5 min at 28 °C
259 using a plate reader (Multiskan FC 3.1; Thermo Fisher Scientific, Inc.) as described previously
260 (Shirai and Yasutomo 2019). The incubation time required to reach a value of 0.25 (OD_{650}) was
261 derived from a regression line during the logarithmic growth phase for each sample.
262
263 **Statistical analysis**
264 All experiments were independently repeated three or four times, and the results are
265 presented as the mean with standard deviation. Statistical analyses were performed using either
266 the two-tailed, unpaired Student's *t*-test (Microsoft Excel 365; Microsoft Corp., Redmond, WA,
267 USA) or one-way analysis of variance (ANOVA) followed by the Tukey-Kramer honest
268 significance difference test for multiple comparisons using Excel Tokei ver. 7.0 software (Esumi
269 Co., Ltd., Tokyo, Japan). P values < 0.05 were considered significant.
270

271 **Results**

272

273 **Photoantifungal effect against yeast cells pre-incubated with FA**

274 As the time of pre-incubation of yeast cells with FA (1 mg ml^{-1}) was extended from 0.5 to 5
275 min, 5-min UV-A exposure yielded a greater reduction in viable cell count (Fig. 1). For a
276 0.5-min pre-incubation, irradiation resulted in a 0.6-log reduction in viability compared with the
277 initial cell count. By comparison, much stronger synergistic photofungicidal activity was
278 observed in samples pre-incubated for 10 min, with a 1.7-log reduction in viable cell count. The
279 following results in particular supported a synergistic effect between FA and UV-A (Fig. S1):
280 yeast cells treated with FA in the absence of UV-A or cells treated with UV-A irradiation only
281 for 10 min exhibited negligible decreases in viability. Following pre-incubation with FA for 5
282 min, UV-A exposure at an irradiance of 19 mW cm^{-2} produced a decrease in viability dependent
283 on irradiation time.

284

285 **Analyses of membrane integrity and SEM investigation of yeast cells**

286 The combination of FA (1 mg ml^{-1}) and UV-A irradiation (5 and 10 min) elicited significant
287 photofungicidal activity, as measured by viable cell count compared with the initial count on the
288 order of 10^7 cells, leading to a 99.8% reduction in viability for a 10-min treatment (Fig. 2A).

289 Additionally, treatment with EPL (100 mg l^{-1}) for 5 or 10 min produced a significant decrease in
290 viability relative to the initial cell count. The reduction in viability after 5 min was almost the
291 same as that observed with combination treatment. Although the survival data obtained with
292 UV-A or FA treatment alone are not shown in the figure, it can be assumed there was no
293 significant change in viability, based on the results shown in Figure S1.

294 The percentage of damaged or dead cells (PI-stained cells) following each treatment is
295 shown in Figures 2B, 2C, and S2. Although combination treatment with a 10-min light exposure
296 increased the number of PI-stained cells by 19%, the treatment did not provide a significant
297 change in the percentage of PI-stained cells compared with the sample before irradiation (0 min).
298 Similarly, there was no significant change in the proportion of PI-stained cells among cells
299 treated with FA alone (in the dark) or cells treated with UV-A alone for the same interval (Fig.
300 S2). In contrast, a clear increase in the proportion of PI-stained cells from 16% to 80% was
301 observed in samples treated with EPL for 10 min compared with the 0-min sample (Fig. 2C).
302 The tendency differed significantly from that of samples treated with the combination.

303 SEM analyses confirmed the photofungicidal action of combined treatment with FA (1 mg
304 ml^{-1}) and 10-min UV-A irradiation. Yeast cells exhibited a comparatively smooth surface after
305 incubation with 0.8% DMSO as a control (without FA and UV-A) and the combination of FA
306 and UV-A treatment, as shown in Figure 2D and E. Cells treated with FA or UV-A irradiation

307 alone also exhibited the same intact morphology as control cells (data not shown). In contrast,
308 cells treated with EPL for the same time exhibited damage, with apparent collapse of the cell
309 surface (Fig. 2F).
310
311 **DNA oxidation**
312 DNA damage was assessed by monitoring the formation of 8-hydroxydeoxyguanosine
313 (8-OHdG), a marker of DNA oxidation, using cells subjected to each treatment for 10 min (Fig.
314 3). A total of 1.13 ng ml^{-1} of 8-OHdG was detected in the control sample (treated in the dark),
315 whereas an 8-OHdG concentration of 0.99 ng ml^{-1} was detected in cells treated with UV-A
316 irradiation alone and 1.14 ng ml^{-1} was detected in cells treated with FA alone. The 8-OHdG
317 concentration was 1.18 ng ml^{-1} in cells treated with combination of FA and UV-A. Therefore,
318 the amount of 8-OHdG formed with the different treatments was almost the same. Data
319 regarding viability after the 10-min combination treatment are shown in Figure 2A.
320
321 **Carbonylation-related damage of cellular proteins and identification of oxidized proteins**
322 To assess carbonylation-related damage of yeast proteins resulting from oxidative reactions,
323 immunoblot analyses were performed using proteins derived from yeast cells treated with FA (1
324 mg ml^{-1}) and UV-A for 3, 5, and 10 min (Fig. 4A). A few protein bands were immunodetected in

325 samples from 3- and 5-min irradiations, but the pattern changed in samples irradiated for 10
326 min; in particular, the overall intensity of the bands decreased. Notably, a reproducibly observed
327 band of approximately 49 kDa was detected, and the intensity of the band increased as the
328 UV-A treatment time extended to 5 min. The other two bands detected, approximately 29 and
329 37 kDa, did not exhibit reproducible increases in the band intensity during 5-min irradiation in
330 four experiments. Figure 4B shows the 49-kDa band intensity for each exposure time, expressed
331 as arbitrary units (a.u.) of mean luminescence normalized to the intensity of samples before
332 UV-A irradiation (0 min). As shown in the figure, combination treatment for only 3 min induced
333 oxidative carbonylation of yeast cell proteins that resulted in a significant 2.0-fold increase in
334 luminescence, and with the 5-min irradiation (causing a 95% reduction in viability; Fig. 2A), the
335 luminescence increased more than 2.3-fold relative to the 0-min samples. However, a
336 non-significant 1.1-fold increase compared with samples before irradiation was observed with
337 samples irradiated for 10 min. On the other hand, any significant increase in the 49-kDa band of
338 carbonylated proteins immunodetected in cells irradiated with UV-A only was difficult to
339 determine based on the minimal change in luminescence (Fig. S3).

340 Proteins derived from yeast cells treated with the combination of FA and UV-A irradiation
341 were separated by 12% SDS-PAGE followed by CBB staining of the gel (Fig. 4C). As indicated
342 by the box in Figure 4C, a band of 50.8 kDa was detected in samples from cells treated with a

343 3-min irradiation. As the molecular mass of this band was close to that of the 49-kDa band
344 detected by immunostaining, it was excised from the gel and subjected to in-gel trypsin
345 digestion, followed by MALDI-TOF MS and database searching using MASCOT Peptide Mass
346 Fingerprint. The protein was identified as PK1 (54.9 kDa) based on high sequence coverage and
347 multiple peptide matches (Tables S1 and S2); the mass spectrum is shown in Figure S4.
348

349 **Effect of FA treatment on intracellular ATP content and cell growth**

350 Figure 5A shows that 3-min treatment of yeast cells with UV-A irradiation alone, FA alone,
351 or combination of FA and UV-A irradiation induced negligible changes in viable cell count
352 compared to treatment without UV-A and FA (control). Figure 5B shows that treatment with FA
353 alone and in combination with UV-A decreased the ATP content to 0.79 ± 0.06 and 0.80 ± 0.09
354 nmol l^{-1}, respectively, corresponding to approximately 77% of the control level. No significant
355 change in ATP content was observed in the sample only irradiated with UV-A as compared to
356 the control.

357 No differences in growth profiles were observed between the control and UV-A–irradiated
358 samples (Fig. S5A). The culture turbidity of yeast cells treated with FA alone or FA combined
359 with irradiation differed markedly from that of control cells or cells treated with irradiation
360 alone, indicating an extension of the lag phase prior to logarithmic growth, namely, a growth

361 delay occurred (Fig. S5B). However, after 70 h of cultivation, the turbidity of all samples
362 reached approximately 1.2 OD_{650}. As the OD_{650} values were >0.1, the values were plotted on a
363 logarithmic scale in Fig. S5C and D. As shown in Table 1, FA treatment in both the absence and
364 presence of UV-A irradiation significantly delayed growth (i.e., time required to reach 0.25
365 OD_{650}): 40.34 ± 1.20 h without irradiation and 39.91 ± 0.71 h with irradiation, compared with
366 the time for control and UV-A samples.
367

368 **Discussion**

369 In this study, we examined the antifungal mechanism of combined treatment with UV-A
370 irradiation and FA, a type of phenolic acid, using *S. cerevisiae*. The photofungicidal effect of the
371 FA and UV-A combination against *Saccharomyces* sp. was similar to the bactericidal efficacy
372 against *E. coli* dependent on UV-A light fluence (Shirai *et al*. 2017). Previous studies examining
373 photobactericidal activity against *E. coli* and *Staphylococcus aureus* found that adsorption of
374 phenolic acids onto the cell surface and their subsequent incorporation into the bacterial
375 membrane plays an important role in mediating the bactericidal effect (Nakamura *et al*. 2015;
376 Shirai and Yasutomo 2019).

377 The photofungicidal activity of phenolic acids such as FA is thought to involve oxidative
378 damage of the cell wall, cytoplasmic membrane, or organelles based on the generation of

379 oxidants such as H_2O_2 and hydroxyl radicals due to reaction between the compounds and light
380 (Nakamura *et al*. 2015; Shirai *et al*. 2015; Nakamura *et al*. 2017). Indeed, addition of catalase
381 and DMSO, which quench ROS, decreased the bactericidal activity of FA and gallic acid,
382 respectively, upon light exposure (Nakamura *et al*. 2012; Shirai *et al*. 2015).

383 The present study observed the generation of H_2O_2 and hydroxyl radicals in FA solution
384 following irradiation, providing clear evidence of FA-mediated ROS production (see Supporting
385 Information Data S1, and Figs. S6 and S7). Inactivation of yeast cells treated with FA under
386 irradiation was diminished dramatically in 10% (v/v) DMSO, a well-known scavenger of
387 hydroxyl radicals (Fig. S8). The generation of hydroxyl radicals *via* photoreactions at the
388 surface or in the interior of yeast cells is thought to affect fungicidal activity due to their high
389 reactivity, as they have a short half-life (estimated ~10^{-9} s) and very short diffusion distance
390 (estimated ~6 nm) (Roots and Okada 1975; Cheng *et al*. 2002). The enhancement of
391 photofungicidal activity by extending the pretreatment time of yeast cells with FA suggests that
392 the adsorption of FA to the cell wall and subsequent incorporation into the cytoplasmic
393 membrane plays an important role in the fungicidal effect in conjunction with the oxidative
394 effects of ROS within the cells.

395 FA induces an increase in the efflux of intracellular ions such as potassium and phosphate,
396 suggesting that it affects the permeability of the bacterial membrane (Campos *et al*. 2009). A

397 study in *E. coli* using flow cytometry analysis of cells stained with PI, which can penetrate
398 damaged cell membranes, revealed that the bactericidal mechanism of FA treatment with UV-A
399 irradiation involves a loss of membrane integrity (Shirai and Yasutomo 2019). The antimicrobial
400 action of the polyphenolic compound curcumin also involves an association with the cell
401 membrane. In another study, when the growth of *Candida* cells treated with curcumin without
402 light irradiation was reduced by 80%, the uptake of PI and morphological changes provided
403 evidence of damage to the cell surface (Kumar *et al*. 2014). In the PACT study of *Botrytis*
404 *cinerea* conidia, a relative increase in intracellular PI levels was induced by applying curcumin
405 to the conidia (Wei *et al*. 2021). However, an investigation of membrane integrity in the present
406 study indicated that cells remained impermeable to PI, even though combination treatment
407 produced a 99.8% reduction in viability. SEM micrographs did not show evidence of major
408 changes on the cell surface. The cationic peptide EPL, a lysine polymer, adsorbs to the bacterial
409 cell membrane due to the molecule's specific electric charge and promotes cell death by
410 destabilizing the membrane (Hyldgaard *et al*. 2014). This compound was employed as a positive
411 control that causes membrane disruption. The percentage of cells that took up PI after treatment
412 with EPL increased to 80% in response to the antifungal activity, suggesting that the integrity of
413 the cell membrane was compromised, as indicated by SEM micrographs showing collapsed
414 cells. Therefore, damage to the cell wall or cytoplasmic membrane does not appear to be the

415 primary fungicidal mechanism of the combination treatment. Moreover, it was presumed that
416 the photofungicidal mechanism differs from the antimicrobial mechanism of photo-activated
417 curcumin, which compromises membrane integrity.

418 Combination treatment using CaA as an FA analogue in conjunction with light irradiation,
419 which can reduce *E. coli* or *S. aureus* viability 5 logs or more, induced the formation of
420 8-OHdG, which is indicative of DNA oxidation in the cells (Nakamura *et al*. 2015). In another
421 study, by contrast, UV-A irradiation of *E. coli* in combination with FA treatment did not result in
422 significant DNA oxidation under conditions yielding a 4.8-log reduction in viability (Shirai and
423 Yasutomo 2019). Combination treatment resulting in a 99.8% reduction in *S. cerevisiae* viability
424 was not associated with an increase in DNA oxidation, and the tendency (i.e., a detectable, but
425 non-significant change in 8-OHdG formation compared with untreated cells) was similar to that
426 observed with *E. coli*. Therefore, adequate disinfection does not result from oxidative DNA
427 damage, which suggests that the photofungicidal system employing FA exhibits low
428 genotoxicity. These results suggest that the photofungicidal effects of FA take place before
429 dysregulation of membrane permeability and DNA oxidation occur.

430 Exposure of *E. coli* cells to lethal UV-A fluence in the logarithmic growth phase generates
431 proteins that are carbonylated due to oxidative modification (Hoerter *et al*. 2005). In contrast,
432 immunostaining after exposure of cells to sublethal UV-A fluence revealed lower total

433 carbonylated protein formation as compared with lethal UV-A irradiation. To elucidate the role
434 of protein oxidation in the observed reduction in viability of *S. cerevisiae* cells subjected to the
435 combination of FA and UV-A, carbonylated proteins were examined by immunodetection
436 followed by proteomics analysis. A significant band of approximately 49 kDa was detected in
437 samples of cells irradiated for up to 5 min in the presence of FA, suggesting that protein
438 oxidation could be associated with the combination-mediated inactivation, which resulted in a
439 95% reduction in viability. The combination treatment decreased the relative intensity levels of
440 proteins detected by immunoblotting and CBB staining of samples from cells subjected to 10
441 min and 5 min of irradiation, respectively. This result could have been due to smearing of
442 protein bands, which is a consequence of covalent cross-linking of proteins, and protein
443 aggregation or fragmentation caused by the excessive oxidation responsible for protein
444 carbonylation (Bosshard *et al*. 2010). Treatment of *E. coli* cells with high UV-A fluence caused
445 the protein bands to smear in immunoblotting and CBB staining. Our supplemental data show
446 that immunodetection of protein damage in yeast cells resulting from excessive oxidative stress
447 decreased with exposure to increasing concentrations of H_2O_2 (Fig. S9).

448 Proteomics analysis of a notable carbonylated protein of ~49 kDa (50.8 kDa by CBB
449 staining of the SDS-PAGE gel) revealed that the protein was a good match to PK1 (54.9 kDa).
450 We hypothesize that this protein is a major target of oxidative stress induced by the combination

451 of FA and UV-A. The cytosolic enzyme PK1 catalyzes the final step in the glycolysis pathway,
452 producing the second of two ATP molecules generated in the pathway (Jurica *et al*. 1998;
453 Enriqueta Muñoz and Ponce 2003). Regulation of the catalytic function of PK1 is important for
454 controlling the levels of ATP, GTP, and glycolytic intermediates such as pyruvate in the cell
455 (Jurica *et al*. 1998). ATP is a vital molecule required in many biological processes, including
456 survival, growth, and replication (Mempin *et al*. 2013). Moreover, intracellular ATP depletion
457 may cause dysfunction of ATP-dependent chaperones, which repair protein misfolding and
458 aggregation. In our study, the ATP content in yeast cells after FA/UV-A photocombination
459 treatment for 3 min decreased to approximately 77% of the control level, despite no significant
460 reduction in viability. Interestingly, treatment with FA alone decreased the ATP content as much
461 as was observed with combination treatment.

462 Compared with non-irradiated cells, *E. coli* cells subjected to sublethal UV-A fluence
463 exhibited delayed growth (Hoerter *et al*. 2005). This growth delay could be attributed to a
464 reduction in the ATP content in the cells caused by protein aggregation or fragmentation after
465 UV-A irradiation, as MS/MS analyses found that many such damaged proteins function in
466 glycolysis and the TCA cycle (Bosshard *et al*. 2010). To verify the effect of reduced ATP levels
467 on biological function, the growth of yeast cells was evaluated. FA-treated cells exhibited
468 delayed growth, which was observed regardless of whether the cells were treated in the dark or

469 with irradiation. A close relationship was found between ATP content and growth rate. However,
470 ATP depletion had a minimal effect on the final turbidity and CFU count.

471 With regard to the changes in cellular function, FA accumulating intracellularly due to
472 adsorption to the cell surface and subsequent translocation across the cytoplasmic membrane
473 could interact with cytosolic proteins such as PK1, thus inducing moderate dysfunction of PK1
474 and a subsequent decrease in intracellular ATP content, leading to the observed delay in growth
475 that preceded inactivation. Results demonstrating that extending the time of pre-incubation with
476 FA enhanced the photofungicidal activity could reflect the accumulation of FA and dysfunction
477 of PK1, from which it is difficult for cells to recover. As shown by the photofungicidal profile,
478 >5-min UV-A irradiation following FA treatment significantly decreased the viable cell count.
479 This result suggests that internally generated ROS resulting from the photoreaction of FA induce
480 irreversible oxidative damage of cytosolic proteins, including PK1, triggering further ATP
481 depletion and ultimately inactivation of the cell. This could be explained by the association
482 between the dependence of total UV-A fluence on exposure time and the amount of ROS
483 generated to completely disrupt the function of cellular proteins. Quantitative analysis using
484 electron spin resonance (ESR) spectrometry revealed that the yield of ROS generated by
485 385-nm UV-A irradiation of CaA depends on the fluence (Nakamura *et al*. 2017). In future
486 studies, it will be necessary to assess whether oxidative stress induced by combinations of FA

487 and UV-A suppresses PK1 activity. The mechanism of action could extend to the membrane and
488 proteins related to the mitochondrial respiratory chain that mediates ATP synthesis, based on
489 results showing that treatment with curcumin or exogenous H_2O_2 exhibiting fungicidal activity
490 associated with oxidative effects induced a collapse of the mitochondrial membrane potential in
491 fungal spores (Qin *et al*. 2011; Wei *et al*. 2021).

492 In conclusion, the results of this study demonstrate the photofungicidal mechanism of
493 combined treatment with FA and UV-A irradiation using *S. cerevisiae*. Our findings suggest that
494 interactions between FA and cytosolic proteins, including PK1, serve as the first step in the
495 fungicidal cascade. These interactions result from the adsorption of FA and its subsequent
496 permeation across the cell wall and cytoplasmic membrane into the cell. This possibility is
497 supported by the observed decrease in viability dependent on the time of pre-incubation with FA
498 and the reduction in ATP content in the presence of FA, which was associated with a markedly
499 reduced growth rate. Irreversible oxidation of proteins occurs in the first stage of the fungicidal
500 action and is caused by the formation of H_2O_2 and hydroxyl radicals by FA-mediated reactions
501 under UV-A irradiation, leading to inactivation of cells. Immunoblotting and proteomics
502 analyses of carbonylated proteins demonstrated oxidative damage to cytosolic proteins,
503 including PK1, which is associated with ATP generation in the glycolysis pathway. In contrast,
504 no significant damage to the cell wall or cytoplasmic membrane was observed based on the

505 impermeability of cells to PI, the lack of morphologic evidence of damage to the cell surface by
506 SEM analysis, and significant oxidative damage to DNA. It is likely that the effect of FA on the
507 cell wall and cytoplasmic membrane of fungal cells when combined with UV-A differs from
508 that of the polyphenolic compound curcumin.
509

510 **Author contributions**

511 A. Shirai designed the study, and A. Shirai, H. Kunimi, and K. Tsuchiya collected the data; A.
512 Shirai wrote the manuscript. All authors have approved the manuscript.
513

514 **Conflict interest**

515 The authors declare that there are no conflicts of interest regarding the publication of this paper.
516

517 **Acknowledgments**

518 We thank JNC Corporation (Tokyo, Japan) for kindly providing ε-polylysine solution (25%).
519 This work did not receive any grants from funding agencies in the public, commercial, or
520 not-for-profit sectors.
521

522 **References**

523 Bernardi, A.O., Stefanello, A., Garcia, M.V., Parussolo, G., Stefanello, R.F., Moro, C.B. and
524 Copetti, M.V. (2018) Efficacy of commercial sanitizers against fungi of concern in the food
525 industry, *LWT* **97** 25-30.
526 Berney, M., Weilenmann, H.U. and Egli, T. (2006) Flow-cytometric study of vital cellular
527 functions in *Escherichia coli* during solar disinfection (SODIS). *Microbiology* **152**,
528 1719-1729.
529 Bosshard, F., Riedel, K., Schneider, T., Geiser, C., Bucheli, M. and Egli, T. (2010) Protein
530 oxidation and aggregation in UVA-irradiated *Escherichia coli* cells as signs of accelerated
531 cellular senescence. *Environ Microbiol* **12**, 2931-2945.
532 Campos, F.M., Couto, J.A., Figueiredo, A.R., Toth, I.V., Rangel, A.O. and Hogg, T.A. (2009)
533 Cell membrane damage induced by phenolic acids on wine lactic acid bacteria. *Int J Food*
534 *Microbiol* **135**, 144-151.
535 Cheng, F.-C., Jen, J.-F. and Tsai, T.-H. (2002) Hydroxyl radical in living systems and its
536 separation methods. *J Chromatogr* **781**, 481–496.
537 Cossu, A., Ercan, D., Wang, Q., Peer, W.A., Nitin, N. and Tikekar, R.V. (2016) Antimicrobial
538 effect of synergistic interaction between UV-A light and gallic acid against *Escherichia coli*
539 O157:H7 in fresh produce wash water and biofilm. *Innov Food Sci Emerg Technol* **37**,
540 44-52.

541 de Oliveira, E.F., Yang, X., Basnayake, N., Huu, C.N., Wang, L., Tikekar, R. and Nitin, N.
542 (2021) Screening of antimicrobial synergism between phenolic acids derivatives and UV-A
543 light radiation. *J Photochem Photobiol B* **214**, 112081.
544 Dovigo, L.N., Pavarina, A.C., Ribeiro, A.P., Brunetti, I.L., Costa, C.A., Jacomassi, D.P.,
545 Bagnato, V.S. and Kurachi, C. (2011) Investigation of the photodynamic effects of curcumin
546 against *Candida albicans*. *Photochem Photobiol* **87**, 895-903.
547 Enriqueta Muñoz, M. and Ponce, E. (2003) Pyruvate kinase: current status of regulatory and
548 functional properties. *Comp Biochem Physiol B Biochem Mol Biol* **135**, 197-218.
549 Hoerter, J.D., Arnold, A.A., Kuczynska, D.A., Shibuya, A., Ward, C.S., Sauer, M.G., Gizachew,
550 A., Hotchkiss, T.M., Fleming, T.J. and Johnson, S. (2005) Effects of sublethal UVA
551 irradiation on activity levels of oxidative defense enzymes and protein oxidation in
552 *Escherichia coli*. *J Photochem Photobiol B* **81**, 171-180.
553 Hyldgaard, M., Mygind, T., Vad, B.S., Stenvang, M., Otzen, D.E. and Meyer, R.L. (2014) The
554 antimicrobial mechanism of action of epsilon-poly-l-lysine. *Appl Environ Microbiol* **80**,
555 7758-7770.
556 Jiang, Y., Leung, A.W., Hua, H., Rao, X. and Xu, C. (2014) Photodynamic action of
557 LED-activated curcumin against *Staphylococcus aureus* involving intracellular ROS
558 increase and membrane damage. *Int J Photoenergy* **2014**, 637601.

559 Jurica, M.S., Mesecar, A., Health, P.J., Shi, W., Nowak, T. and Stoddard, B.L. (1998) The
560 allosteric regulation of pyruvate kinase by fructose-1,6-bisphosphate. *Structure* **6**, 195-210.
561 Krisch, J., Chandrasekaran, M., Kadaikunnan, S., Alharbi, N.S. and Vagvolgyi, C. (2016) Latest
562 about spoilage by yeasts: Focus on the deterioration of beverages and other plant-derived
563 products. *J Food Prot* **79**, 825-829.
564 Kumar, A., Dhamgaye, S., Maurya, I.K., Singh, A., Sharma, M. and Prasad, R. (2014) Curcumin
565 targets cell wall integrity via calcineurin-mediated signaling in *Candida albicans*.
566 *Antimicrob Agents Chemother* **58**, 167-175.
567 Kumar, N. and Pruthi, V. (2014) Potential applications of ferulic acid from natural sources.
568 *Biotechnol Rep* **4**, 86-93.
569 Mempin, R., Tran, H., Chen, C., Gong, H., Ho, K.-K. and Lu, S. (2013) Release of extracellular
570 ATP by bacteria during growth. *BMC Microbiol* **13**, 301.
571 Nakamura, K., Ishiyama, K., Sheng, H., Ikai, H., Kanno, T. and Niwano, Y. (2015) Bactericidal
572 activity and mechanism of photoirradiated polyphenols against gram-positive and -negative
573 bacteria. *J Agric Food Chem* **63**, 7707-7713.
574 Nakamura, K., Shirato, M., Kanno, T., Lingstrom, P., Ortengren, U. and Niwano, Y. (2017)
575 Photo-irradiated caffeic acid exhibits antimicrobial activity against *Streptococcus mutans*
576 biofilms via hydroxyl radical formation. *Sci Rep* **7**, 6353.

577 Nakamura, K., Yamada, Y., Ikai, H., Kanno, T., Sasaki, K. and Niwano, Y. (2012) Bactericidal
578 action of photoirradiated gallic acid via reactive oxygen species formation. *J Agric Food*
579 *Chem* **60**, 10048-10054.
580 Paiva, L.B.d., Goldbeck, R., Santos, W.D.d. and Squina, F.M. (2013) Ferulic acid and
581 derivatives molecules with potential application in the pharmaceutical field. *Braz J Pharm*
582 *Sci* **49**, 395-411.
583 Qin, G., Liu, J., Cao, B., Li, B. and Tian, S. (2011) Hydrogen peroxide acts on sensitive
584 mitochondrial proteins to induce death of a fungal pathogen revealed by proteomic analysis.
585 *PLoS One* **6**, e21945.
586 Roots, R. and Okada, S. (1975) Estimation of life times and diffusion distances of radicals
587 involved in X-ray-induced DNA strand breaks or killing of mammalian cells. *Radiat Res* **64**,
588 306-320.
589 Rosazza, J.P.N., Huang, Z., Dostal, L., Volm, T. and Rousseau, B. (1995) Review: Biocatalytic
590 transformations of ferulic acid: an abundant aromatic natural product. *J Ind Microbiol* **15**,
591 457-471.
592 Shirai, A., Aihara, M., Takahashi, A., Maseda, H. and Omasa, T. (2014) Synergistic
593 antimicrobial activity based on the combined use of a gemini-quaternary ammonium
594 compound and ultraviolet-A light. *J Photochem Photobiol B* **130**, 226-233.

595 Shirai, A., Kajiura, M. and Omasa, T. (2015) Synergistic photobactericidal activity based on
596 ultraviolet-A irradiation and ferulic acid derivatives. *Photochem Photobiol* **91**, 1422-1428.
597 Shirai, A., Sumitomo, T., Kurimoto, M., Maseda, H. and Kourai, H. (2009) The mode of the
598 antifungal activity of gemini-pyridinium salt against yeast. *Biocontol Sci* **14**, 13-20.
599 Shirai, A., Watanabe, T. and Matsuki, H. (2017) Inactivation of foodborne pathogenic and
600 spoilage micro-organisms using ultraviolet-A light in combination with ferulic acid. *Lett*
601 *Appl Microbiol* **64**, 96-102.
602 Shirai, A. and Yasutomo, Y. (2019) Bactericidal action of ferulic acid with ultraviolet-A light
603 irradiation. *J Photochem Photobiol B* **191**, 52-58.
604 Temba, B.A., Fletcher, M.T., Fox, G.P., Harvey, J.J.W. and Sultanbawa, Y. (2016) Inactivation
605 of *Aspergillus flavus* spores by curcumin-mediated photosensitization. *Food Control* **59**,
606 708-713.
607 Wei, C., Zhang, F., Song, L., Chen, X. and Meng, X. (2021) Photosensitization effect of
608 curcumin for controlling plant pathogen *Botrytis cinerea* in postharvest apple. *Food Control*
609 **123**, 107683.
610 Zabka, M. and Pavela, R. (2013) Antifungal efficacy of some natural phenolic compounds
611 against significant pathogenic and toxinogenic filamentous fungi. *Chemosphere* **93**,
612 1051-1056.
613

614

615

616 **Table 1** Effect of treatment with FA and UV-A irradiation on time required to reach 0.25 OD_{650}.

Incubation time (h)*			
Incubation alone	Irradiation alone	FA alone	FA + irradiation
25.70 ± 0.30[a]	24.20 ± 0.21[a]	40.34 ± 1.20[b]	39.91 ± 0.71[b]

617 *Incubation time was derived from the regression line during the logarithmic growth phase for

618 each sample and is indicated as the time required to reach 0.25 OD_{650} (see Fig. S5). Data are

619 presented as the mean ± SD (n=4). Different letters refer to significant differences between

620 groups ($P < 0.01$; one-way ANOVA).

621 **Figure legends**

622 Fig. 1. Effect of pre-incubation with FA on photofungicidal activity with a 5-min UV-A
623 irradiation of *S. cerevisiae* cells. Each cell suspension (initial density, 2-3 × 10^5 CFU ml^{-1}) was
624 pre-incubated for 0.5 to 10 min, followed by irradiation at an irradiance of 19 mW cm^{-2} for 5
625 min. Data are presented as the mean ± SD (n=3). Different letters above the bars denote
626 significant differences between groups ($P < 0.05$; one-way ANOVA).

627

628 Fig. 2. Analysis of *S. cerevisiae* cellular functions after treatment with three indicators. Panel A
629 shows the inactivation level of the cells after each treatment: open circles, combination of 1 mg
630 ml^{-1} FA and UV-A; shaded squares, 100 mg l^{-1} EPL. Panels B and C show the percentage of
631 PI-stained cells among 10,000 cells treated with the combination and EPL, respectively. Data
632 are presented as the mean ± SD (n=3). Panels D-F show SEM images of cells after each
633 treatment: D, control (0.8% DMSO) for 10 min; E, combination for 10 min; F, EPL for 10 min.
634 All micrographs are shown at a magnification of ×20,000. White scale bars represent 2 μm.
635 Significant differences compared to the initial for each sample (by two-tailed, unpaired *t*-test)
636 are indicated as follows: $^{+}P < 0.05$, $^{**}P < 0.01$, and *** and $^{+++}P < 0.001$. ns, not significant.

637

638 Fig. 3. DNA oxidation in *S. cerevisiae* after each treatment. Yeast cell suspension (initial density,

639 2-3 × 10^7 CFU ml^{-1}) was treated with FA and UV-A. Data are presented as the mean ± SD (n=3).

640 Identical letters above the bars denote no significant difference between the groups (one-way

641 ANOVA).

642

643 Fig. 4. Oxidative damage of proteins in *S. cerevisiae* treated with the combination of 1 mg ml^{-1}

644 FA and UV-A irradiation at an irradiance of 19 mW cm^{-2}: A, immunodetection of carbonylated

645 proteins; B, luminescence level of the band at ~49 kDa immunodetected as shown in panel A,

646 expressed as arbitrary units (a.u.) of mean luminescence normalized to the signal of samples

647 before UV-A irradiation (0 min). Data are presented as the mean ± SD (n=4). Panel C shows

648 staining of proteins with CBB to monitor samples after combination treatment. MALDI-TOF

649 MS determined proteins including the band (50.8 kDa) surrounded with a box in the figure (see

650 Fig. S4, and Tables S1 and S2). Different letters above the bars denote significant differences

651 between groups ($P < 0.01$ and only $P < 0.05$ between 3- and 10-min samples; one-way

652 ANOVA).

653

654 Fig. 5. Effect of treatment with FA and UV-A light irradiation on ATP content in *S. cerevisiae*

655 cells. Viable cell count after each treatment is shown in panel A. The ATP content correlating

656 with each treatment is shown in panel B. Data are presented as the mean ± SD (n=3). Different

657 letters above the bars denote significant differences between groups ($P < 0.05$; one-way

658 ANOVA).

659

660 **Supporting Information**

661 The following are the Supplementary Data associated with this article: Data S1, Tables S1 and

662 S2, and Figures S1 to S9.

663

664 Data S1. Determination of light-generated hydrogen peroxide and hydroxyl radicals

665

666 Table S1. MALDI-TOF MS identification of *S. cerevisiae* proteins affected by treatment with

667 FA and UV-A irradiation.

668

669 Table S2. Score and matched peptides of the protein identified by MALDI-TOF MS.

670

671 Fig. S1. Time-course analysis of changes in the inactivation of *S. cerevisiae* after each treatment.

672 Initial cells were suspended at a density of 2-3 × 10^5 CFU ml^{-1}. UV-A irradiance was set at 19

673 mW cm^{-2}. Symbols: UV-A irradiation alone (open squares); 1 mg ml^{-1} FA alone (in the dark,

674 shaded circles); combination of 1 mg ml^{-1} FA and UV-A irradiation (open circles). Data are

675 presented as means ± SD (n=3). Significant differences (**P < 0.01 and ***P < 0.001;

676 two-tailed, unpaired *t*-test) were determined based on comparison with initial viability.

677

678 Fig. S2. Dual-parameter dot plots of 10,000 double-stained cells (Cyto 9 and PI) evaluated by

679 flow cytometry after incubation for 0 min (A, upper line) or 5 min (B, lower line). Upper and

680 lower squares indicate PI- (damage or dead) and Cyto 9–stained cells (live), respectively. The

681 numbers near squares in each panel indicate the percentage of live cells and damaged or dead

682 cells among a total of 10,000 cells.

683

684 Fig. S3. Oxidative damage of cellular proteins in *S. cerevisiae* treated with UV-A alone at an

685 irradiance of 19 mW cm^{-2}: luminescence levels of the band at ~49 kDa (A) and of proteins (B)

686 immunodetected on Western blots, expressed as arbitrary units (a.u.) of mean luminescence

687 normalized to the signal levels of samples before UV-A irradiation (0 min). Data are presented

688 as the mean ± SD (n=3). Identical letters above the bars indicate no significant differences

689 between groups (one-way ANOVA).

690

691 Fig. S4. MALDI-TOF mass spectrum of the peptide produced by in-gel tryptic digestion.

692

693 Fig. S5. Effect of treatment with FA and UV-A irradiation on *S. cerevisiae* growth. Growth in

694 each sample was monitored by measuring the optical density at 650 nm (OD_{650}) in panels A and

695 B. As the OD_{650} values were >0.1, the values were plotted on a logarithmic scale in panels C and

696 D. Graphs show growth curves for each sample in the absence (A and C) or presence (B and D)

697 of FA. Lines in all figures indicate samples without (solid lines) and with (dotted lines) UV-A

698 irradiation. Values are presented as the mean (n=4).

699

700 Fig. S6. Concentration of H_2O_2 generated in FA solution with and without UV-A light

701 irradiation. Left and right (open) bars for each treatment indicate H_2O_2 concentration after

702 incubation for 30 min in the dark or UV-A exposure at an irradiance of 4.77 mW cm^{-2},

703 respectively. Data are presented as means ± SD (n=3). Significant differences (***$P < 0.001$;

704 two-tailed, unpaired *t*-test). Cont., sample without FA; nd, not detected.

705

706 Fig. S7. Formation of 5,5-dimethyl-1-pyrroline-*N*-oxide (DMPO)/$^{\bullet}$OH adducts in solutions

707 containing phenolic acids before and after irradiation. ESR spectra of mixtures of 4.5 mmol l^{-1}

708 FA and 450 mmol l^{-1} DMPO were recorded before and after irradiation with UV-A light (4.77

709 mW cm^{-2}) for 3 min. The control sample consisted of 450 mmol l^{-1} DMPO solution prepared

710 with pure water alone. Each figure shows the ESR spectrum for pure water (A and C) and FA (B

711 and D) before (A and B) and after (C and D) irradiation. Values in the figure indicate signal

712 intensity of the second line of the DMPO/$^{\bullet}$OH adduct graphs (arbitrary units).

713

714 Fig. S8. Effect of DMSO on inactivation of *S. cerevisiae*. Conidia suspensions (initial density,

715 2-3 × 10^5 CFU ml^{-1}) were exposed to UV-A irradiation at an irradiance of 19 mW cm^{-2} for 10

716 min after addition of FA at a concentration of 1 mg ml^{-1} followed by addition of DMSO. Data

717 are presented as the mean ± SD (n=3). ***$P < 0.001$; two-tailed, unpaired *t*-test.

718

719 Fig. S9. Oxidative damage of cellular proteins in *S. cerevisiae* (initial density, 2-3 × 10^7 CFU

720 ml^{-1}) treated with H_2O_2 at a concentration of 0.02 to 0.5% for 20 min. Luminescence levels of

721 proteins immunodetected on Western blots, expressed as arbitrary units (a.u.) of mean

722 luminescence normalized to the signal levels of untreated samples. Data are presented as the

723 mean ± SD (n=3). Different letters above the bars denote significant differences between the

724 groups ($P < 0.05$; one-way ANOVA).

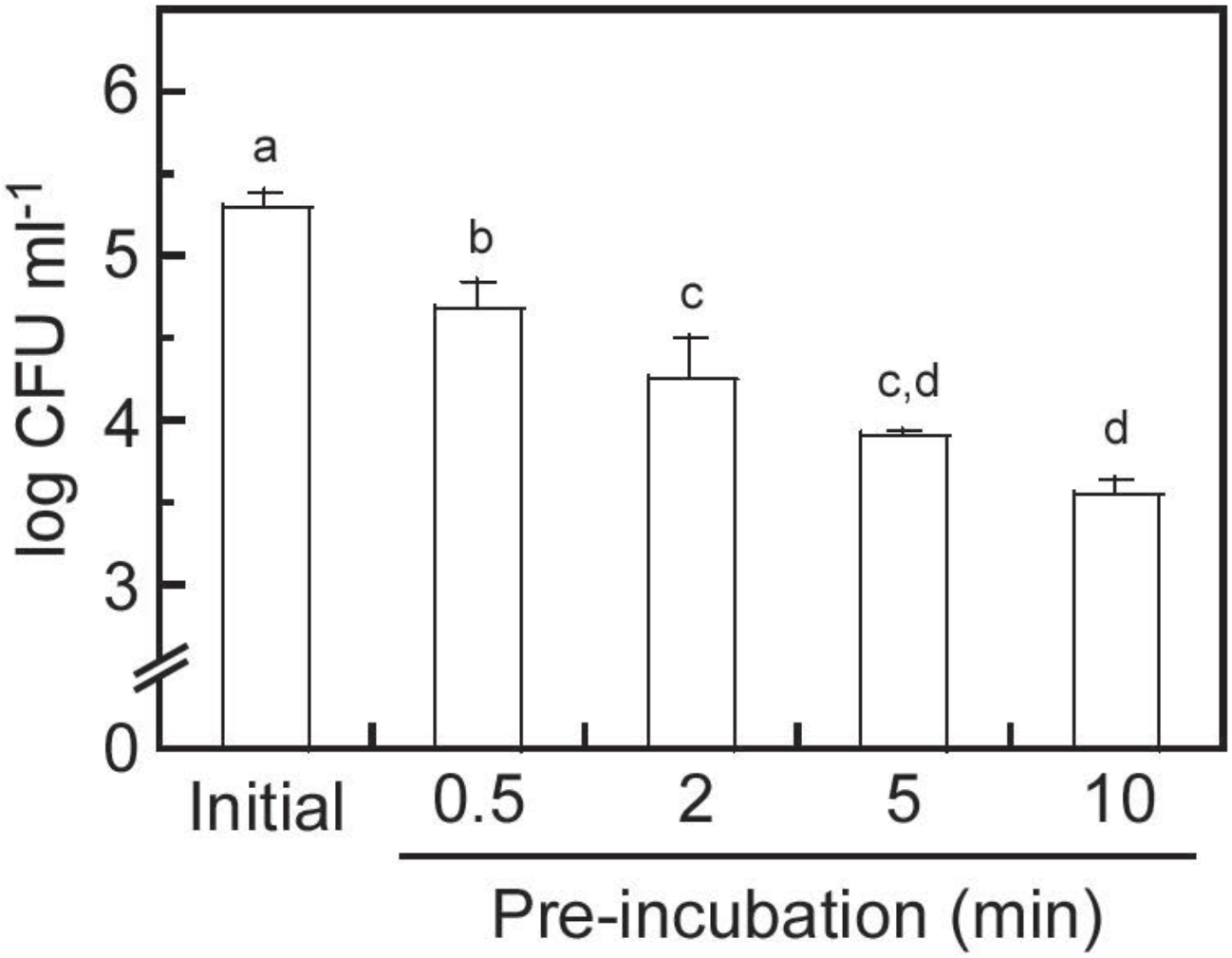

Fig.1 Effect of pre-incubation with FA on photofungicidal activity with a 5-min UV-A irradiation of *S. cerevisiae* cells. Each cell suspension (initial density, 2-3 $\times$ 10^5 CFU ml^{-1}) was pre-incubated for 0.5 to 10 min, followed by irradiation at an irradiance of 19 mW cm^{-2} for 5 min. Data are presented as the mean $\pm$ SD (n=3). Different letters above the bars denote significant differences between groups ($P <$ 0.05; one-way ANOVA).

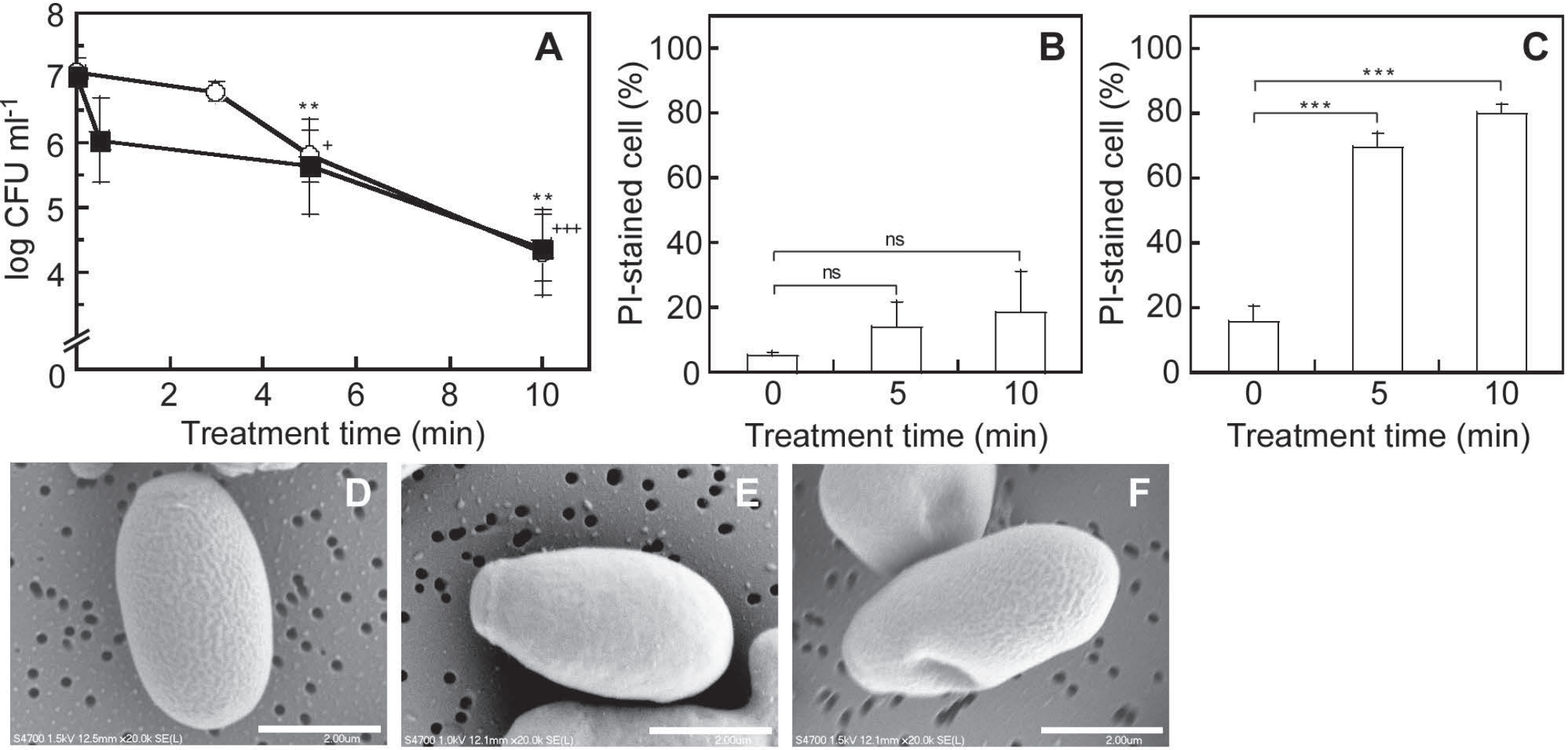

Fig. 2 Analysis of *S. cerevisiae* cellular functions after treatment with three indicators. Panel A shows the inactivation level of the cells after each treatment: open circles, combination of 1 mg ml^{-1} FA and UV-A; shaded squares, 100 mg l^{-1} EPL. Panels B and C show the percentage of PI-stained cells among 10,000 cells treated with the combination and EPL, respectively. Data are presented as the mean ± SD (n=3). Panels D-F show SEM images of cells after each treatment: D, control (0.8% DMSO) for 10 min; E, combination for 10 min; F, EPL for 10 min. All micrographs are shown at a magnification of ×20,000. White scale bars represent 2 μm. Significant differences compared to the initial for each sample (by two-tailed, unpaired *t*-test) are indicated as follows: $^{+}P < 0.05$, $^{**}P < 0.01$, and *** and $^{+++}P < 0.001$. ns, not significant.

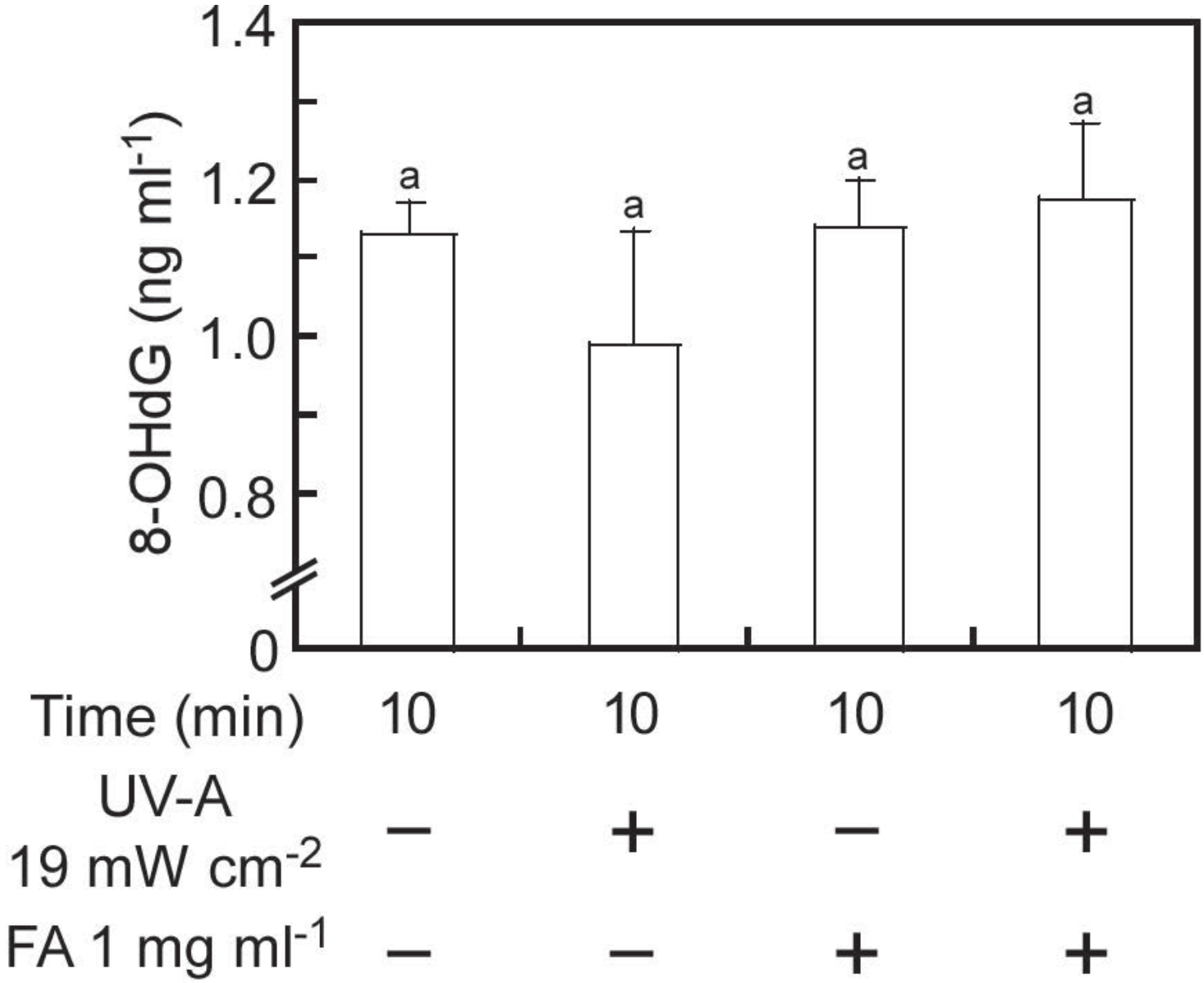

Fig. 3 DNA oxidation in *S. cerevisiae* after each treatment. Yeast cell suspension (initial density, 2-3 $\times$ 10^7 CFU ml^{-1}) was treated with FA and UV-A. Data are presented as the mean $\pm$ SD (n=3). Identical letters above the bars denote no significant difference between the groups (one-way ANOVA).

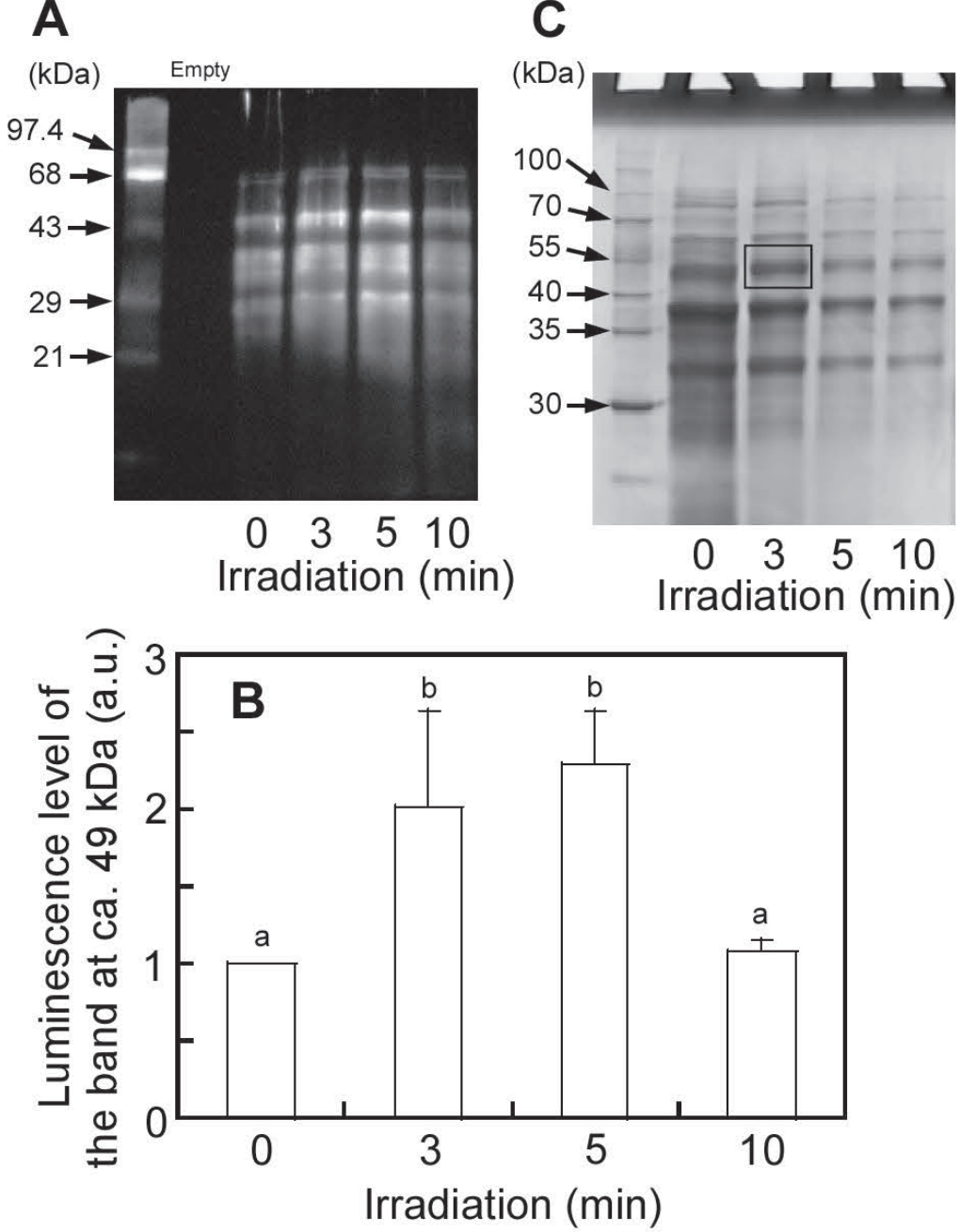

Fig. 4 Oxidative damage of proteins in *S. cerevisiae* treated with the combination of 1 mg ml^{-1} FA and UV-A irradiation at an irradiance of 19 mW cm^{-2}: A, immunodetection of carbonylated proteins; B, luminescence level of the band at ~49 kDa immunodetected as shown in panel A, expressed as arbitrary units (a.u.) of mean luminescence normalized to the signal of samples before UV-A irradiation (0 min). Data are presented as the mean ± SD (n=4). Panel C shows staining of proteins with CBB to monitor samples after combination treatment. MALDI-TOF MS determined proteins including the band (50.8 kDa) surrounded with a box in the figure (see Fig. S4 and Table S1). Different letters above the bars denote significant differences between groups ($P < 0.01$ and only $P < 0.05$ between 3- and 10-min samples; one-way ANOVA).

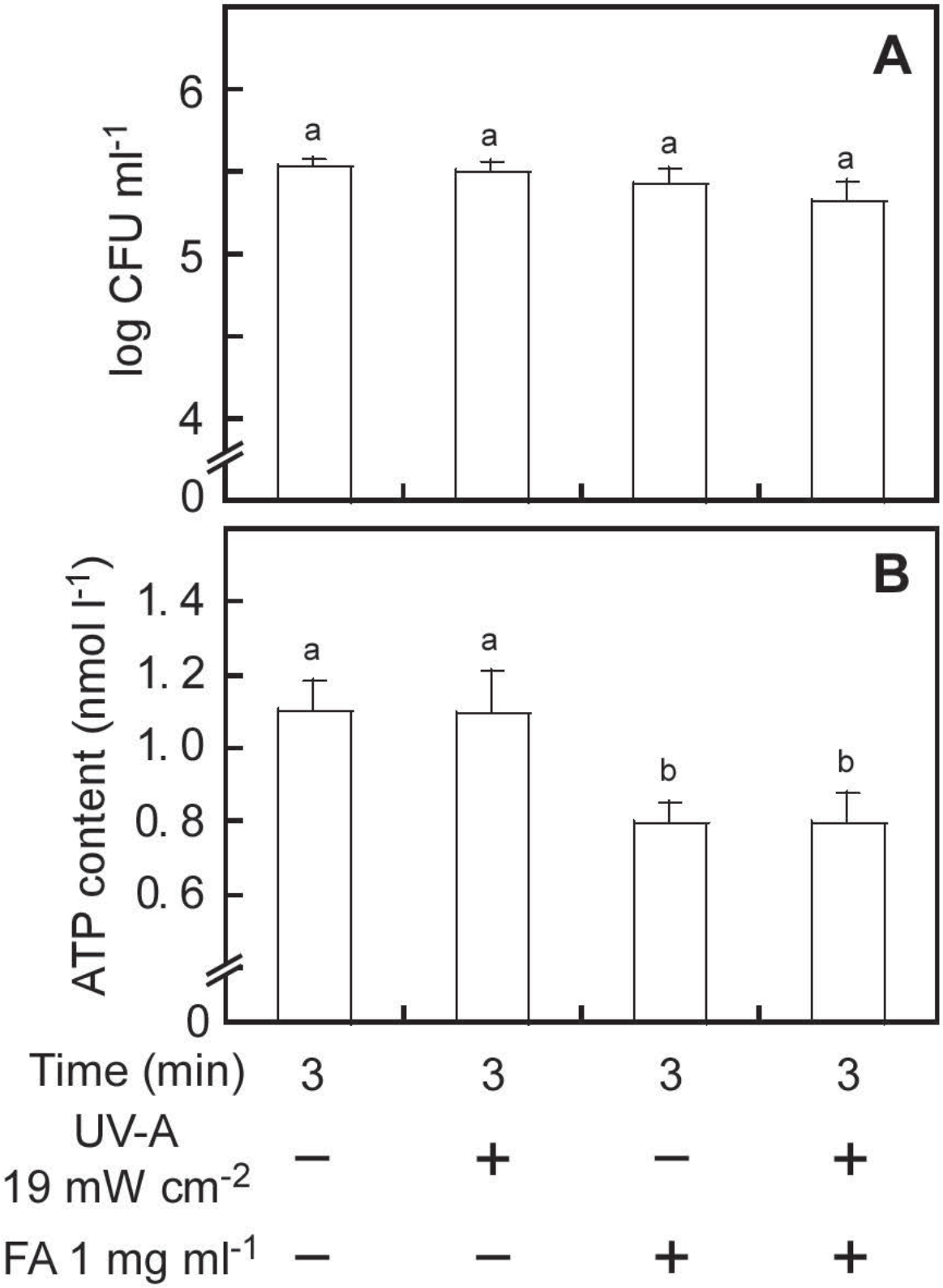

Fig. 5 Effect of treatment with FA and UV-A light irradiation on ATP content in *S. cerevisiae* cells. Viable cell count after each treatment is shown in panel A. The ATP content correlating with each treatment is shown in panel B. Data are presented as the mean ± SD (n=3). Different letters above the bars denote significant differences between groups ($P < 0.05$; one-way ANOVA).

Data S1

Title

Antifungal action of the combination of ferulic acid and ultraviolet-A irradiation against *Saccharomyces cerevisiae*

Author names

A. Shirai [1, 2], H. Kunimi [3] and K. Tsuchiya [4]

Affiliations

[1] Department of Bioscience and Bioindustry, Graduate School of Technology, Industrial and Social Sciences, Tokushima University, 2-1 Minami-Josanjima, Tokushima 770-8513, Japan.

[2] Institute of Post-LED Photonics, Tokushima University, 2-1 Minami-Josanjima, Tokushima 770-8506, Japan.

[3] Graduate School of Advanced Technology and Science, Tokushima University, 2-1 Minami-Josanjima, Tokushima 770-8506, Japan.

[4] Department of Medical Pharmacology, Institute of Biomedical Sciences, Graduate School of Tokushima University, 1-78-1 Sho-machi, Tokushima 770-8505, Japan.

*Corresponding author: Akihiro Shirai

Department of Bioscience and Bioindustry, Graduate School of Technology, Industrial and Social Sciences, Tokushima University, 2-1 Minami-Josanjima, Tokushima 770-8506, Japan.

e-mail: a.shirai@tokushima-u.ac.jp

Determination of light-generated hydrogen peroxide and hydroxyl radicals

One milliliter of FA solution (1 mg ml^{-1}) prepared with pure water (Hikari Pharmaceutical Co., Ltd., Tokyo, Japan) was added to a well of a 24-well culture plate (AGC Tecno Glass Co., Ltd., Tokyo, Japan) and irradiated at 4.77 mW cm^{-2} for 30 min in an incubator box at 25°C. Measurement of H_2O_2 was conducted by a colorimetric method using xylenol orange according to the protocol described by Nakamura *et al*. (2015). After reaction with xylenol orange, the absorbance of the mixture was measured using a UV-Vis spectrophotometer (UV-1850; Shimadzu Corp., Kyoto, Japan). The concentration of H_2O_2 was calculated using a standard curve over a concentration range of 0.2 to 5.0 μmol l^{-1}. The detection limit for the assay was 0.4 μmol l^{-1}.

Generation of H_2O_2 was observed in irradiated sample solutions (Fig. S6). Significantly, the concentration of H_2O_2 generated in FA solution, 3.05 μmol l^{-1}, was 6.5-fold higher than that of the

37 sample treated with irradiation alone (control). Furthermore, H_2O_2 concentrations were generally

38 below the detection limit (0.4 μmol l^{-1}) in non-irradiated samples.

39 Hydroxyl radicals were detected by a quick reaction with the nitrone spin trap reagent 5,5-

40 dimethyl-1-pyrroline-*N*-oxide (DMPO) using an electron spin resonance (ESR) spectrometer

41 (EMXPlus, Bruker Corp., Billerica, MA, USA) with an X-band cavity (ER 4103TM, Bruker

42 Corp.) (Finkelstein *et al*. 1980; Tsuda *et al*. 2018). The ESR spectra of reaction mixtures of 4.5

43 mmol l^{-1} (0.87 mg ml^{-1}) FA and 450 mmol l^{-1} DMPO in a quartz flat cell (250 μl) were recorded

44 on the apparatus before and after irradiation with UV-A light (4.77 mW cm^{-2}) for 3 min. Pure

45 water was also prepared for control samples with or without light exposure. The quartz cell was

46 set into the ESR spectrometer. Hyperfine coupling constants were obtained using the computer

47 program Winsim (version 0.96; NIEHS, NIH, Research Triangle Park, NC, USA,

48 https://www.niehs.nih.gov) (Duling 1994). The measurement conditions for ESR were as follows:

49 microwave frequency of 9.8497 GHz, microwave power of 10 mW, sweep width of 3505 ± 50

50 gauss, modulation frequency of 100 kHz, modulation amplitude of 1.0 gauss, time constant of

51 164 ms, and conversion time of 230 ms.

52 The ESR spectra (Fig. S7) indicated that no signal was detected for pure water and the FA

53 solution before irradiation (panels A and B). Typical ESR signals were clearly detected in the FA

54 solution after UV-A light exposure compared with the irradiated control sample (panels C and D).

55 The signal was determined to be an DMPO/$^{\bullet}$OH adduct, a spin adduct of the hydroxyl radical,

56 from the hyperfine coupling constants ($a^N = a^H = 1.49$ mT) (Rosen and Rauckman 1981).

57 Therefore, ESR analysis demonstrated the generation of hydroxyl radicals mediated by FA under

58 UV-A light exposure.

59

60 **References**

61

62 Duling, D.R. (1994) Simulation of multiple isotropic spin-trap EPR spectra. *J Magn Reson B* **104**,

63 105-110.

64 Finkelstein, E., Rosen, G.M. and Rauckman, E.J. (1980) Spin trapping of superoxide and

65 hydroxyl radical: practical aspects. *Arch Biochem Biophys* **200**, 1-16.

66 Nakamura, K., Ishiyama, K., Sheng, H., Ikai, H., Kanno, T. and Niwano, Y. (2015) Bactericidal

67 activity and mechanism of photoirradiated polyphenols against gram-positive and -negative

68 bacteria. *J Agric Food Chem* **63**, 7707-7713.

69 Rosen, G.M. and Rauckman, E.J. (1981) Spin trapping of free radicals during hepatic microsomal

70 lipid peroxidation. *Proc Natl Acad Sci U S A* **78**, 7346-7349.

71 Tsuda, K., Miyamoto, L., Hamano, S., Morimoto, Y., Kangawa, Y., Fukue, C., Kagawa, Y.,

72 Horinouchi, Y., Xu, W., Ikeda, Y., Tamaki, T. and Tsuchiya, K. (2018) Mechanisms of the pH-

73 and oxygen-dependent oxidation activities of artesunate. *Biol Pharm Bull* **41**, 555-563.

Table S1 MALDI-TOF MS identification of *S. cerevisiae* proteins affected by treatment with FA and UV-A irradiation[*].

Accession number[**]	Protein name and function[+]	Theo. *Mr* (kDa)/pI[++]	Expt. *Mr* (kDa)[#]	Species[##]	Mascot Score[§]	NP[§§]	Expect[¶]	SC (%)[¶¶]
P00549	Pyruvate kinase 1 Glycolysis	54.9/7.59	50.8	*S. cerevisiae*	109	15	1e-07	45
Q12506	Uncharacterized protein	12.7/7.66	50.8	*S. cerevisiae*	52	5	0.052	75

[*]For details, refer to Table S2.

[**]Accession number from UniProt database of a matched protein.

[+]Protein function defined by the UniProt database.

[++]Theoretical molecular mass and isoelectric point based on amino acid sequence of the identified protein.

[#]Experimental molecular mass and isoelectric point estimated from the SDS-PAGE gel shown in Figure 4C.

[##]Species of the matched protein.

[§]Score obtained from Mascot for each match. Mascot scores >51 are significant ($P < 0.05$).

[§§]Number of unique peptides identified.

[¶]Expected value.

[¶¶]Protein sequence coverage.

Table S2-1 Score and matched peptides of the protein identified by MALDI-TOF MS

Mascot Score Histogram
Protein score is -10*Log(P), where P is the probability that the observed match is a random event.
Protein scores greater than 51 are significant (p<0.05).

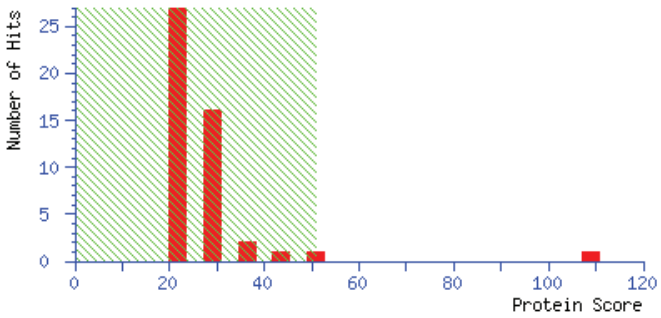

Protein View: KPYK1_YEAST
Pyruvate kinase 1 OS=Saccharomyces cerevisiae (strain ATCC 204508 / S288c) OX=559292 GN=CDC19 PE=1 SV=2

Database:	SwissProt
Score:	109
Expect:	1.00E-07
Monoisotopic mass (Mr):	54909
Calculated pI:	7.56
Taxonomy:	Saccharomyces cerevisiae S288C

Sequence similarity is available as an NCBI BLAST search of KPYK1_YEAST against nr.

Search parameters
Enzyme:
Trypsin: cuts C-term side of KR unless next residue is P.

Fixed modifications:	Carbamidomethyl (C)
Mass values searched:	79
Mass values matched:	15

Protein sequence coverage: 45%

Matched peptides shown in ***bold red***.

1 MSRLER**LTSL** **NVVAGSDLRR** **TSIIGTIGPK** **TNNPETLVAL** **RKAGLNIVR**M
51 NFSHGSYEYH KSVIDNAR**KS** **EELYPGRPLA** **IALDTK**GPEI R**TGTTTNDVD**

101	**YPIPPNHEMI**	**FTTDDKYAK**A	CDDKIMYVDY	KNITKVISAG	RIIYVDDGVL
151	SFQVLEVVDD	KTLKVKALNA	GKICSHKGVN	LPGTDVDLPA	LSEKDKEDLR
201	FGVKNGVHMV	FASFIR**TAND**	**VLTIR**EVLGE	QGKDVKIIVK	**IENQQGVNNF**
251	**DEILKVTDGV**	**MVAR**GDLGIE	IPAPEVLAVQ	KKLIAK**SNLA**	**GKPVICATQM**
301	**LESMTYNPRP**	**TRAEVSDVGN**	**AILDGADCVM**	**LSGETAK**GNY	PINAVTTMAE
351	TAVIAEQAIA	YLPNYDDMRN	CTPKPTSTTE	TVAASAVAAV	FEQKAK**AIIV**
401	**LSTSGTTPR**L	VSK**YRPNCPI**	**ILVTR**CPRAA	R**FSHLYRGVF**	**PFVFEKEPVS**
451	**DWTDDVEAR**I	NFGIEKAKEF	GILKKGDTYV	SIQGFKAGAG	HSNTLQVSTV

Start	–	End	Observed	Mr(expt)	Mr(calc)	ppm	M	Peptide
7	–	20	1500.8374	1499.8301	1499.842	-7.9	1	R.LTSLNVVAGSDLRR.T
20	–	30	1142.6994	1141.6921	1141.6819	8.96	1	R.RTSIIGTIGPK.T
31	–	41	1227.6765	1226.6692	1226.6619	5.99	0	K.TNNPETLVALR.K
31	–	42	1355.7551	1354.7478	1354.7568	-6.65	1	K.TNNPETLVALRK.A
42	–	49	870.5316	869.5243	869.5447	-23.4	1	R.KAGLNIVR.M
69	–	86	2001.0642	2000.0569	2000.0942	-18.6	1	R.KSEELYPGRPLAIALDTK.G
92	–	119	3184.8682	3183.8609	3183.4707	123	1	R.TGTTTNDVDYPIPPNHEMIFTTDDKYAK.A
217	–	225	1002.5642	1001.5569	1001.5506	6.36	0	R.TANDVLTIR.E
241	–	264	2689.4215	2688.4142	2688.3541	22.4	1	K.IENQQGVNNFDEILKVTDGVMVAR.G
287	–	312	2935.6587	2934.6514	2934.4514	68.2	0	K.SNLAGKPVICATQMLESMTYNPRPTR.A
313	–	337	2522.3599	2521.3526	2521.1676	73.4	0	R.AEVSDVGNAILDGADCVMLSGETAK.G
397	–	409	1315.7586	1314.7513	1314.7507	0.46	0	K.AIIVLSTSGTTPR.L
414	–	425	1501.8166	1500.8093	1500.8235	-9.44	0	K.YRPNCPIILVTR.C
432	–	437	822.393	821.3857	821.4184	-39.8	0	R.FSHLYR.G
438	–	459	2569.2564	2568.2491	2568.2173	12.4	1	R.GVFPFVFEKEPVSDWTDDVEAR.I

```
ID   KPYK1_YEAST          Reviewed;        500 AA.
AC   P00549; D6VPH8; Q2VQG5;
DT   21-JUL-1986, integrated into UniProtKB/Swiss-Prot.
DT   01-JUL-1989, sequence version 2.
DT   07-APR-2021, entry version 216.
DE   RecName: Full=Pyruvate kinase 1;
DE          Short=PK 1;
DE          EC=2.7.1.40 {ECO:0000269|PubMed:10413488};
DE   AltName: Full=cell division cycle protein 19;
GN   Name=CDC19; Synonyms=PYK1; OrderedLocusNames=YAL038W;
OS   Saccharomyces cerevisiae (strain ATCC 204508 / S288c) (Baker's yeast).
OC   Eukaryota; Fungi; Dikarya; Ascomycota; Saccharomycotina; Saccharomycetes;
OC   Saccharomycetales; Saccharomycetaceae; Saccharomyces.
OX   NCBI_TaxID=559292;
```

RN [1]
RP NUCLEOTIDE SEQUENCE [GENOMIC DNA].
RX PubMed=2653861; DOI=10.1016/0014-5793(89)81359-6;
RA McNally T., Purvis I.J., Fothergill-Gilmore L.A., Brown A.L.P.;
RT "The yeast pyruvate kinase gene does not contain a string of non-preferred
RT codons: revised nucleotide sequence.";
RL FEBS Lett. 247:312-316(1989).
RN [2]
RP NUCLEOTIDE SEQUENCE [GENOMIC DNA].
RX PubMed=6185493;
RA Burke R.L., Tekamp-Olson P., Najarian R.;
RT "The isolation, characterization, and sequence of the pyruvate kinase gene
RT of Saccharomyces cerevisiae.";
RL J. Biol. Chem. 258:2193-2201(1983).
RN [3]
RP NUCLEOTIDE SEQUENCE [GENOMIC DNA].
RC STRAIN=ATCC 76625 / YPH499, Ba194, Bb32, Fy93, M1-2A, M2-8, M5-7A, M5-7B,
RC M7-8D, MMR2-1, MMR2-3, MMR2-5, MMW1-12, MMW1-15, MMW1-15h2, MMW1-2,
RC MMW1-2h2, ORM1-1, Sgu52E, Sgu52F, YPS396, YPS400, YPS598, YPS600, YPS602,
RC YPS604, YPS606, YPS608, and YPS610;
RX PubMed=16879422; DOI=10.1111/j.1567-1364.2006.00059.x;
RA Aa E., Townsend J.P., Adams R.I., Nielsen K.M., Taylor J.W.;
RT "Population structure and gene evolution in Saccharomyces cerevisiae.";
RL FEMS Yeast Res. 6:702-715(2006).
RN [4]
RP NUCLEOTIDE SEQUENCE [LARGE SCALE GENOMIC DNA].
RC STRAIN=ATCC 204508 / S288c;
RX PubMed=7731988; DOI=10.1073/pnas.92.9.3809;
RA Bussey H., Kaback D.B., Zhong W.-W., Vo D.H., Clark M.W., Fortin N.,
RA Hall J., Ouellette B.F.F., Keng T., Barton A.B., Su Y., Davies C.J.,
RA Storms R.K.;
RT "The nucleotide sequence of chromosome I from Saccharomyces cerevisiae.";
RL Proc. Natl. Acad. Sci. U.S.A. 92:3809-3813(1995).
RN [5]
RP GENOME REANNOTATION.
RC STRAIN=ATCC 204508 / S288c;
RX PubMed=24374639; DOI=10.1534/g3.113.008995;
RA Engel S.R., Dietrich F.S., Fisk D.G., Binkley G., Balakrishnan R.,
RA Costanzo M.C., Dwight S.S., Hitz B.C., Karra K., Nash R.S., Weng S.,
RA Wong E.D., Lloyd P., Skrzypek M.S., Miyasato S.R., Simison M., Cherry J.M.;
RT "The reference genome sequence of Saccharomyces cerevisiae: Then and now.";
RL G3 (Bethesda) 4:389-398(2014).
RN [6]

RP NUCLEOTIDE SEQUENCE [GENOMIC DNA].
RC STRAIN=ATCC 204508 / S288c;
RX PubMed=17322287; DOI=10.1101/gr.6037607;
RA Hu Y., Rolfs A., Bhullar B., Murthy T.V.S., Zhu C., Berger M.F.,
RA Camargo A.A., Kelley F., McCarron S., Jepson D., Richardson A., Raphael J.,
RA Moreira D., Taycher E., Zuo D., Mohr S., Kane M.F., Williamson J.,
RA Simpson A.J.G., Bulyk M.L., Harlow E., Marsischky G., Kolodner R.D.,
RA LaBaer J.;
RT "Approaching a complete repository of sequence-verified protein-encoding
RT clones for Saccharomyces cerevisiae.";
RL Genome Res. 17:536-543(2007).
RN [7]
RP CATALYTIC ACTIVITY, COFACTOR, BIOPHYSICOCHEMICAL PROPERTIES, AND
RP MUTAGENESIS OF LYS-240.
RX PubMed=10413488; DOI=10.1021/bi990690n;
RA Bollenbach T.J., Mesecar A.D., Nowak T.;
RT "Role of lysine 240 in the mechanism of yeast pyruvate kinase catalysis.";
RL Biochemistry 38:9137-9145(1999).
RN [8]
RP LEVEL OF PROTEIN EXPRESSION [LARGE SCALE ANALYSIS].
RX PubMed=14562106; DOI=10.1038/nature02046;
RA Ghaemmaghami S., Huh W.-K., Bower K., Howson R.W., Belle A., Dephoure N.,
RA O'Shea E.K., Weissman J.S.;
RT "Global analysis of protein expression in yeast.";
RL Nature 425:737-741(2003).
RN [9]
RP IDENTIFICATION BY MASS SPECTROMETRY [LARGE SCALE ANALYSIS].
RC STRAIN=YAL6B;
RX PubMed=15665377; DOI=10.1074/mcp.m400219-mcp200;
RA Gruhler A., Olsen J.V., Mohammed S., Mortensen P., Faergeman N.J., Mann M.,
RA Jensen O.N.;
RT "Quantitative phosphoproteomics applied to the yeast pheromone signaling
RT pathway.";
RL Mol. Cell. Proteomics 4:310-327(2005).
RN [10]
RP PHOSPHORYLATION [LARGE SCALE ANALYSIS] AT SER-9 AND THR-478, AND
RP IDENTIFICATION BY MASS SPECTROMETRY [LARGE SCALE ANALYSIS].
RC STRAIN=ADR376;
RX PubMed=17330950; DOI=10.1021/pr060559j;
RA Li X., Gerber S.A., Rudner A.D., Beausoleil S.A., Haas W., Villen J.,
RA Elias J.E., Gygi S.P.;
RT "Large-scale phosphorylation analysis of alpha-factor-arrested
RT Saccharomyces cerevisiae.";

RL J. Proteome Res. 6:1190-1197(2007).
RN [11]
RP ACETYLATION [LARGE SCALE ANALYSIS] AT SER-2, PHOSPHORYLATION [LARGE SCALE
RP ANALYSIS] AT SER-213, CLEAVAGE OF INITIATOR METHIONINE [LARGE SCALE
RP ANALYSIS], AND IDENTIFICATION BY MASS SPECTROMETRY [LARGE SCALE ANALYSIS].
RX PubMed=17287358; DOI=10.1073/pnas.0607084104;
RA Chi A., Huttenhower C., Geer L.Y., Coon J.J., Syka J.E.P., Bai D.L.,
RA Shabanowitz J., Burke D.J., Troyanskaya O.G., Hunt D.F.;
RT "Analysis of phosphorylation sites on proteins from Saccharomyces
RT cerevisiae by electron transfer dissociation (ETD) mass spectrometry.";
RL Proc. Natl. Acad. Sci. U.S.A. 104:2193-2198(2007).
RN [12]
RP PHOSPHORYLATION [LARGE SCALE ANALYSIS] AT SER-16, AND IDENTIFICATION BY
RP MASS SPECTROMETRY [LARGE SCALE ANALYSIS].
RX PubMed=18407956; DOI=10.1074/mcp.m700468-mcp200;
RA Albuquerque C.P., Smolka M.B., Payne S.H., Bafna V., Eng J., Zhou H.;
RT "A multidimensional chromatography technology for in-depth phosphoproteome
RT analysis.";
RL Mol. Cell. Proteomics 7:1389-1396(2008).
RN [13]
RP PHOSPHORYLATION [LARGE SCALE ANALYSIS] AT SER-9; SER-16; THR-31; SER-70;
RP THR-184; SER-316; SER-450 AND THR-478, AND IDENTIFICATION BY MASS
RP SPECTROMETRY [LARGE SCALE ANALYSIS].
RX PubMed=19779198; DOI=10.1126/science.1172867;
RA Holt L.J., Tuch B.B., Villen J., Johnson A.D., Gygi S.P., Morgan D.O.;
RT "Global analysis of Cdk1 substrate phosphorylation sites provides insights
RT into evolution.";
RL Science 325:1682-1686(2009).
RN [14]
RP UBIQUITINATION [LARGE SCALE ANALYSIS] AT LYS-204; LYS-255 AND LYS-446, AND
RP IDENTIFICATION BY MASS SPECTROMETRY [LARGE SCALE ANALYSIS].
RX PubMed=22106047; DOI=10.1002/pmic.201100166;
RA Starita L.M., Lo R.S., Eng J.K., von Haller P.D., Fields S.;
RT "Sites of ubiquitin attachment in Saccharomyces cerevisiae.";
RL Proteomics 12:236-240(2012).
RN [15]
RP X-RAY CRYSTALLOGRAPHY (3.00 ANGSTROMS) IN COMPLEX WITH SUBSTRATE ANALOG;
RP FRUCTOSE-1-6-DIPHOSPHATE; MANGANESE IONS AND POTASSIUM IONS.
RX PubMed=9519410; DOI=10.1016/s0969-2126(98)00021-5;
RA Jurica M.S., Mesecar A., Heath P.J., Shi W., Nowak T., Stoddard B.L.;
RT "The allosteric regulation of pyruvate kinase by fructose-1,6-
RT bisphosphate.";
RL Structure 6:195-210(1998).

```
CC   -!- CATALYTIC ACTIVITY:
CC       Reaction=ATP + pyruvate = ADP + H(+) + phosphoenolpyruvate;
CC         Xref=Rhea:RHEA:18157, ChEBI:CHEBI:15361, ChEBI:CHEBI:15378,
CC         ChEBI:CHEBI:30616, ChEBI:CHEBI:58702, ChEBI:CHEBI:456216;
CC         EC=2.7.1.40; Evidence={ECO:0000269|PubMed:10413488};
CC   -!- COFACTOR:
CC       Name=Mg(2+); Xref=ChEBI:CHEBI:18420;
CC         Evidence={ECO:0000269|PubMed:10413488};
CC   -!- COFACTOR:
CC       Name=K(+); Xref=ChEBI:CHEBI:29103;
CC         Evidence={ECO:0000305|PubMed:9519410};
CC   -!- ACTIVITY REGULATION: The activity is regulated by glucose levels.
CC       Activated by fructose-1,6-bisphosphate.
CC   -!- BIOPHYSICOCHEMICAL PROPERTIES:
CC       Kinetic parameters:
CC         KM=0.31 mM for phosphoenolpyruvate (with magnesium as divalent
CC         cation) {ECO:0000269|PubMed:10413488};
CC         KM=0.021 mM for phosphoenolpyruvate (with manganese as divalent
CC         cation) {ECO:0000269|PubMed:10413488};
CC         KM=1.10 mM for ADP (with magnesium as divalent cation)
CC         {ECO:0000269|PubMed:10413488};
CC         KM=0.24 mM for ADP (with manganese as divalent cation)
CC         {ECO:0000269|PubMed:10413488};
CC       pH dependence:
CC         Optimum pH is 6.0. {ECO:0000269|PubMed:10413488};
CC   -!- PATHWAY: Carbohydrate degradation; glycolysis; pyruvate from D-
CC       glyceraldehyde 3-phosphate: step 5/5.
CC   -!- SUBUNIT: Homotetramer.
CC   -!- MISCELLANEOUS: Present with 291000 molecules/cell in log phase SD
CC       medium. {ECO:0000269|PubMed:14562106}.
CC   -!- SIMILARITY: Belongs to the pyruvate kinase family. {ECO:0000305}.
CC   ---------------------------------------------------------------------------
CC   Copyrighted by the UniProt Consortium, see https://www.uniprot.org/terms
CC   Distributed under the Creative Commons Attribution (CC BY 4.0) License
CC   ---------------------------------------------------------------------------
DR   EMBL; V01321; CAA24631.1; -; Genomic_DNA.
DR   EMBL; X14400; CAA32573.1; -; Genomic_DNA.
DR   EMBL; AY949862; AAY27264.1; -; Genomic_DNA.
DR   EMBL; AY949863; AAY27265.1; -; Genomic_DNA.
DR   EMBL; AY949864; AAY27266.1; -; Genomic_DNA.
DR   EMBL; AY949865; AAY27267.1; -; Genomic_DNA.
DR   EMBL; AY949866; AAY27268.1; -; Genomic_DNA.
DR   EMBL; AY949867; AAY27269.1; -; Genomic_DNA.
```

DR EMBL; AY949868; AAY27270.1; -; Genomic_DNA.
DR EMBL; AY949869; AAY27271.1; -; Genomic_DNA.
DR EMBL; AY949870; AAY27272.1; -; Genomic_DNA.
DR EMBL; AY949871; AAY27273.1; -; Genomic_DNA.
DR EMBL; AY949872; AAY27274.1; -; Genomic_DNA.
DR EMBL; AY949873; AAY27275.1; -; Genomic_DNA.
DR EMBL; AY949874; AAY27276.1; -; Genomic_DNA.
DR EMBL; AY949875; AAY27277.1; -; Genomic_DNA.
DR EMBL; AY949876; AAY27278.1; -; Genomic_DNA.
DR EMBL; AY949877; AAY27279.1; -; Genomic_DNA.
DR EMBL; AY949878; AAY27280.1; -; Genomic_DNA.
DR EMBL; AY949879; AAY27281.1; -; Genomic_DNA.
DR EMBL; AY949880; AAY27282.1; -; Genomic_DNA.
DR EMBL; AY949881; AAY27283.1; -; Genomic_DNA.
DR EMBL; AY949882; AAY27284.1; -; Genomic_DNA.
DR EMBL; AY949883; AAY27285.1; -; Genomic_DNA.
DR EMBL; AY949884; AAY27286.1; -; Genomic_DNA.
DR EMBL; AY949885; AAY27287.1; -; Genomic_DNA.
DR EMBL; AY949886; AAY27288.1; -; Genomic_DNA.
DR EMBL; AY949887; AAY27289.1; -; Genomic_DNA.
DR EMBL; AY949888; AAY27290.1; -; Genomic_DNA.
DR EMBL; AY949889; AAY27291.1; -; Genomic_DNA.
DR EMBL; AY949890; AAY27292.1; -; Genomic_DNA.
DR EMBL; U12980; AAC04993.1; -; Genomic_DNA.
DR EMBL; AY693107; AAT93126.1; -; Genomic_DNA.
DR EMBL; BK006935; DAA06948.1; -; Genomic_DNA.
DR PIR; S05764; KIBYP.
DR RefSeq; NP_009362.1; NM_001178183.1.
DR PDB; 1A3W; X-ray; 3.00 A; A/B=1-500.
DR PDB; 1A3X; X-ray; 3.00 A; A/B=1-500.
DR PDBsum; 1A3W; -.
DR PDBsum; 1A3X; -.
DR SMR; P00549; -.
DR BioGRID; 31727; 293.
DR DIP; DIP-4124N; -.
DR ELM; P00549; -.
DR IntAct; P00549; 186.
DR MINT; P00549; -.
DR STRING; 4932.YAL038W; -.
DR MoonProt; P00549; -.
DR CarbonylDB; P00549; -.
DR iPTMnet; P00549; -.
DR COMPLUYEAST-2DPAGE; P00549; -.

DR MaxQB; P00549; -.
DR PaxDb; P00549; -.
DR PRIDE; P00549; -.
DR TopDownProteomics; P00549; -.
DR EnsemblFungi; YAL038W_mRNA; YAL038W; YAL038W.
DR GeneID; 851193; -.
DR KEGG; sce:YAL038W; -.
DR SGD; S000000036; CDC19.
DR VEuPathDB; FungiDB:YAL038W; -.
DR eggNOG; KOG2323; Eukaryota.
DR GeneTree; ENSGT00390000008859; -.
DR HOGENOM; CLU_015439_0_1_1; -.
DR InParanoid; P00549; -.
DR OMA; QVPIVQK; -.
DR Reactome; R-SCE-6798695; Neutrophil degranulation.
DR Reactome; R-SCE-70171; Glycolysis.
DR SABIO-RK; P00549; -.
DR UniPathway; UPA00109; UER00188.
DR EvolutionaryTrace; P00549; -.
DR PRO; PR:P00549; -.
DR Proteomes; UP000002311; Chromosome I.
DR RNAct; P00549; protein.
DR GO; GO:0005737; C:cytoplasm; IDA:SGD.
DR GO; GO:0005886; C:plasma membrane; HDA:SGD.
DR GO; GO:0005524; F:ATP binding; IEA:UniProtKB-KW.
DR GO; GO:0016301; F:kinase activity; IEA:UniProtKB-KW.
DR GO; GO:0000287; F:magnesium ion binding; IEA:InterPro.
DR GO; GO:0030955; F:potassium ion binding; IEA:InterPro.
DR GO; GO:0004743; F:pyruvate kinase activity; IDA:SGD.
DR GO; GO:0006096; P:glycolytic process; IMP:SGD.
DR GO; GO:0006090; P:pyruvate metabolic process; IMP:SGD.
DR CDD; cd00288; Pyruvate_Kinase; 1.
DR Gene3D; 2.40.33.10; -; 1.
DR Gene3D; 3.20.20.60; -; 1.
DR Gene3D; 3.40.1380.20; -; 1.
DR InterPro; IPR001697; Pyr_Knase.
DR InterPro; IPR015813; Pyrv/PenolPyrv_Kinase-like_dom.
DR InterPro; IPR040442; Pyrv_Kinase-like_dom_sf.
DR InterPro; IPR011037; Pyrv_Knase-like_insert_dom_sf.
DR InterPro; IPR018209; Pyrv_Knase_AS.
DR InterPro; IPR015793; Pyrv_Knase_brl.
DR InterPro; IPR015795; Pyrv_Knase_C.
DR InterPro; IPR036918; Pyrv_Knase_C_sf.

```
DR   InterPro; IPR015806; Pyrv_Knase_insert_dom_sf.
DR   PANTHER; PTHR11817; PTHR11817; 1.
DR   Pfam; PF00224; PK; 1.
DR   Pfam; PF02887; PK_C; 1.
DR   PRINTS; PR01050; PYRUVTKNASE.
DR   SUPFAM; SSF50800; SSF50800; 1.
DR   SUPFAM; SSF51621; SSF51621; 1.
DR   SUPFAM; SSF52935; SSF52935; 1.
DR   TIGRFAMs; TIGR01064; pyruv_kin; 1.
DR   PROSITE; PS00110; PYRUVATE_KINASE; 1.
PE   1: Evidence at protein level;
KW   3D-structure; Acetylation; Allosteric enzyme; ATP-binding; Glycolysis;
KW   Isopeptide bond; Kinase; Magnesium; Manganese; Metal-binding;
KW   Nucleotide-binding; Phosphoprotein; Potassium; Pyruvate;
KW   Reference proteome; Transferase; Ubl conjugation.
FT   INIT_MET        1
FT                   /note="Removed"
FT                   /evidence="ECO:0007744|PubMed:17287358"
FT   CHAIN           2..500
FT                   /note="Pyruvate kinase 1"
FT                   /id="PRO_0000112121"
FT   NP_BIND         51..54
FT                   /note="ATP"
FT                   /evidence="ECO:0000250|UniProtKB:P14618"
FT   REGION          402..407
FT                   /note="FBP binding; allosteric activator"
FT                   /evidence="ECO:0000269|PubMed:9519410,
FT                   ECO:0007744|PDB:1A3W"
FT   METAL           51
FT                   /note="Potassium"
FT                   /evidence="ECO:0000269|PubMed:9519410,
FT                   ECO:0007744|PDB:1A3W, ECO:0007744|PDB:1A3X"
FT   METAL           53
FT                   /note="Potassium"
FT                   /evidence="ECO:0000269|PubMed:9519410,
FT                   ECO:0007744|PDB:1A3W, ECO:0007744|PDB:1A3X"
FT   METAL           84
FT                   /note="Potassium"
FT                   /evidence="ECO:0000269|PubMed:9519410,
FT                   ECO:0007744|PDB:1A3W, ECO:0007744|PDB:1A3X"
FT   METAL           85
FT                   /note="Potassium; via carbonyl oxygen"
FT                   /evidence="ECO:0000269|PubMed:9519410,
```

```
FT                   ECO:0007744|PDB:1A3W, ECO:0007744|PDB:1A3X"
FT   METAL           242
FT                   /note="Manganese"
FT                   /evidence="ECO:0000269|PubMed:9519410,
FT                   ECO:0007744|PDB:1A3W, ECO:0007744|PDB:1A3X"
FT   METAL           266
FT                   /note="Manganese"
FT                   /evidence="ECO:0000269|PubMed:9519410,
FT                   ECO:0007744|PDB:1A3W, ECO:0007744|PDB:1A3X"
FT   BINDING         49
FT                   /note="Substrate"
FT                   /evidence="ECO:0000269|PubMed:9519410,
FT                   ECO:0007744|PDB:1A3X"
FT   BINDING         91
FT                   /note="ATP"
FT                   /evidence="ECO:0000250|UniProtKB:P14618"
FT   BINDING         177
FT                   /note="ATP"
FT                   /evidence="ECO:0000250|UniProtKB:P14618"
FT   BINDING         240
FT                   /note="Substrate; via amide nitrogen"
FT                   /evidence="ECO:0000269|PubMed:9519410,
FT                   ECO:0007744|PDB:1A3X"
FT   BINDING         265
FT                   /note="Substrate; via amide nitrogen"
FT                   /evidence="ECO:0000269|PubMed:9519410,
FT                   ECO:0007744|PDB:1A3W, ECO:0007744|PDB:1A3X"
FT   BINDING         266
FT                   /note="Substrate; via amide nitrogen"
FT                   /evidence="ECO:0000269|PubMed:9519410,
FT                   ECO:0007744|PDB:1A3W"
FT   BINDING         298
FT                   /note="Substrate"
FT                   /evidence="ECO:0000269|PubMed:9519410,
FT                   ECO:0007744|PDB:1A3W, ECO:0007744|PDB:1A3X"
FT   BINDING         452
FT                   /note="FBP; allosteric activator"
FT                   /evidence="ECO:0000269|PubMed:9519410,
FT                   ECO:0007744|PDB:1A3W, ECO:0007744|PDB:1A3X"
FT   BINDING         459
FT                   /note="FBP; allosteric activator"
FT                   /evidence="ECO:0000269|PubMed:9519410,
FT                   ECO:0007744|PDB:1A3W, ECO:0007744|PDB:1A3X"
```

```
FT   BINDING         484
FT                   /note="FBP; allosteric activator; via amide nitrogen"
FT                   /evidence="ECO:0000269|PubMed:9519410,
FT                   ECO:0007744|PDB:1A3W, ECO:0007744|PDB:1A3X"
FT   SITE            240
FT                   /note="Transition state stabilizer"
FT                   /evidence="ECO:0000269|PubMed:10413488"
FT   MOD_RES         2
FT                   /note="N-acetylserine"
FT                   /evidence="ECO:0007744|PubMed:17287358"
FT   MOD_RES         9
FT                   /note="Phosphoserine"
FT                   /evidence="ECO:0007744|PubMed:17330950,
FT                   ECO:0007744|PubMed:19779198"
FT   MOD_RES         16
FT                   /note="Phosphoserine"
FT                   /evidence="ECO:0007744|PubMed:18407956,
FT                   ECO:0007744|PubMed:19779198"
FT   MOD_RES         31
FT                   /note="Phosphothreonine"
FT                   /evidence="ECO:0007744|PubMed:19779198"
FT   MOD_RES         70
FT                   /note="Phosphoserine"
FT                   /evidence="ECO:0007744|PubMed:19779198"
FT   MOD_RES         184
FT                   /note="Phosphothreonine"
FT                   /evidence="ECO:0007744|PubMed:19779198"
FT   MOD_RES         213
FT                   /note="Phosphoserine"
FT                   /evidence="ECO:0007744|PubMed:17287358"
FT   MOD_RES         316
FT                   /note="Phosphoserine"
FT                   /evidence="ECO:0007744|PubMed:19779198"
FT   MOD_RES         450
FT                   /note="Phosphoserine"
FT                   /evidence="ECO:0007744|PubMed:19779198"
FT   MOD_RES         478
FT                   /note="Phosphothreonine"
FT                   /evidence="ECO:0007744|PubMed:17330950,
FT                   ECO:0007744|PubMed:19779198"
FT   CROSSLNK        204
FT                   /note="Glycyl lysine isopeptide (Lys-Gly) (interchain with
FT                   G-Cter in ubiquitin)"
```

```
FT                   /evidence="ECO:0007744|PubMed:22106047"
FT   CROSSLNK        255
FT                   /note="Glycyl lysine isopeptide (Lys-Gly) (interchain with
FT                   G-Cter in ubiquitin)"
FT                   /evidence="ECO:0007744|PubMed:22106047"
FT   CROSSLNK        446
FT                   /note="Glycyl lysine isopeptide (Lys-Gly) (interchain with
FT                   G-Cter in ubiquitin)"
FT                   /evidence="ECO:0007744|PubMed:22106047"
FT   MUTAGEN         240
FT                   /note="K->M: Reduces activity 1000-fold."
FT                   /evidence="ECO:0000269|PubMed:10413488"
FT   CONFLICT        382..386
FT                   /note="VAASA -> SLPR (in Ref. 1; CAA24631)"
FT                   /evidence="ECO:0000305"
FT   HELIX           3..8
FT                   /evidence="ECO:0007744|PDB:1A3W"
FT   STRAND          21..26
FT                   /evidence="ECO:0007744|PDB:1A3X"
FT   HELIX           29..31
FT                   /evidence="ECO:0007744|PDB:1A3W"
FT   HELIX           34..43
FT                   /evidence="ECO:0007744|PDB:1A3W"
FT   STRAND          47..49
FT                   /evidence="ECO:0007744|PDB:1A3W"
FT   HELIX           57..73
FT                   /evidence="ECO:0007744|PDB:1A3W"
FT   STRAND          82..84
FT                   /evidence="ECO:0007744|PDB:1A3W"
FT   STRAND          96..99
FT                   /evidence="ECO:0007744|PDB:1A3W"
FT   STRAND          108..112
FT                   /evidence="ECO:0007744|PDB:1A3W"
FT   TURN            116..120
FT                   /evidence="ECO:0007744|PDB:1A3W"
FT   STRAND          126..129
FT                   /evidence="ECO:0007744|PDB:1A3W"
FT   HELIX           133..136
FT                   /evidence="ECO:0007744|PDB:1A3W"
FT   STRAND          142..145
FT                   /evidence="ECO:0007744|PDB:1A3W"
FT   TURN            146..149
FT                   /evidence="ECO:0007744|PDB:1A3W"
```

```
FT   STRAND         150..153
FT                  /evidence="ECO:0007744|PDB:1A3W"
FT   TURN           159..161
FT                  /evidence="ECO:0007744|PDB:1A3X"
FT   STRAND         163..167
FT                  /evidence="ECO:0007744|PDB:1A3W"
FT   STRAND         178..180
FT                  /evidence="ECO:0007744|PDB:1A3W"
FT   HELIX          193..205
FT                  /evidence="ECO:0007744|PDB:1A3W"
FT   STRAND         208..212
FT                  /evidence="ECO:0007744|PDB:1A3W"
FT   HELIX          218..232
FT                  /evidence="ECO:0007744|PDB:1A3W"
FT   STRAND         235..241
FT                  /evidence="ECO:0007744|PDB:1A3W"
FT   HELIX          245..248
FT                  /evidence="ECO:0007744|PDB:1A3W"
FT   HELIX          250..256
FT                  /evidence="ECO:0007744|PDB:1A3W"
FT   STRAND         260..262
FT                  /evidence="ECO:0007744|PDB:1A3W"
FT   HELIX          264..270
FT                  /evidence="ECO:0007744|PDB:1A3W"
FT   HELIX          273..275
FT                  /evidence="ECO:0007744|PDB:1A3W"
FT   HELIX          276..290
FT                  /evidence="ECO:0007744|PDB:1A3W"
FT   STRAND         294..296
FT                  /evidence="ECO:0007744|PDB:1A3W"
FT   HELIX          302..305
FT                  /evidence="ECO:0007744|PDB:1A3W"
FT   HELIX          312..324
FT                  /evidence="ECO:0007744|PDB:1A3W"
FT   STRAND         327..329
FT                  /evidence="ECO:0007744|PDB:1A3W"
FT   TURN           333..337
FT                  /evidence="ECO:0007744|PDB:1A3W"
FT   HELIX          341..355
FT                  /evidence="ECO:0007744|PDB:1A3W"
FT   STRAND         357..359
FT                  /evidence="ECO:0007744|PDB:1A3X"
FT   HELIX          361..368
```

```
FT                   /evidence="ECO:0007744|PDB:1A3W"
FT   HELIX           378..393
FT                   /evidence="ECO:0007744|PDB:1A3W"
FT   STRAND          398..401
FT                   /evidence="ECO:0007744|PDB:1A3W"
FT   STRAND          403..405
FT                   /evidence="ECO:0007744|PDB:1A3W"
FT   HELIX           406..413
FT                   /evidence="ECO:0007744|PDB:1A3W"
FT   STRAND          420..425
FT                   /evidence="ECO:0007744|PDB:1A3W"
FT   HELIX           429..432
FT                   /evidence="ECO:0007744|PDB:1A3W"
FT   HELIX           433..435
FT                   /evidence="ECO:0007744|PDB:1A3W"
FT   STRAND          439..443
FT                   /evidence="ECO:0007744|PDB:1A3W"
FT   TURN            452..454
FT                   /evidence="ECO:0007744|PDB:1A3W"
FT   HELIX           455..469
FT                   /evidence="ECO:0007744|PDB:1A3W"
FT   STRAND          478..483
FT                   /evidence="ECO:0007744|PDB:1A3W"
FT   TURN            487..489
FT                   /evidence="ECO:0007744|PDB:1A3W"
FT   STRAND          494..499
FT                   /evidence="ECO:0007744|PDB:1A3W"
SQ   SEQUENCE   500 AA;  54545 MW;  78D753FC410C5820 CRC64;
     MSRLERLTSL NVVAGSDLRR TSIIGTIGPK TNNPETLVAL RKAGLNIVRM NFSHGSYEYH
     KSVIDNARKS EELYPGRPLA IALDTKGPEI RTGTTTNDVD YPIPPNHEMI FTTDDKYAKA
     CDDKIMYVDY KNITKVISAG RIIYVDDGVL SFQVLEVVDD KTLKVKALNA GKICSHKGVN
     LPGTDVDLPA LSEKDKEDLR FGVKNGVHMV FASFIRTAND VLTIREVLGE QGKDVKIIVK
     IENQQGVNNF DEILKVTDGV MVARGDLGIE IPAPEVLAVQ KKLIAKSNLA GKPVICATQM
     LESMTYNPRP TRAEVSDVGN AILDGADCVM LSGETAKGNY PINAVTTMAE TAVIAEQAIA
     YLPNYDDMRN CTPKPTSTTE TVAASAVAAV FEQKAKAIIV LSTSGTTPRL VSKYRPNCPI
     ILVTRCPRAA RFSHLYRGVF PFVFEKEPVS DWTDDVEARI NFGIEKAKEF GILKKGDTYV
     SIQGFKAGAG HSNTLQVSTV
```

Table S2-2 Score and matched peptides of the protein identified by MALDI-TOF MS

Mascot Score Histogram
Protein score is -10*Log(P), where P is the probability that the observed match is a random event.
Protein scores greater than 51 are significant (p<0.05).

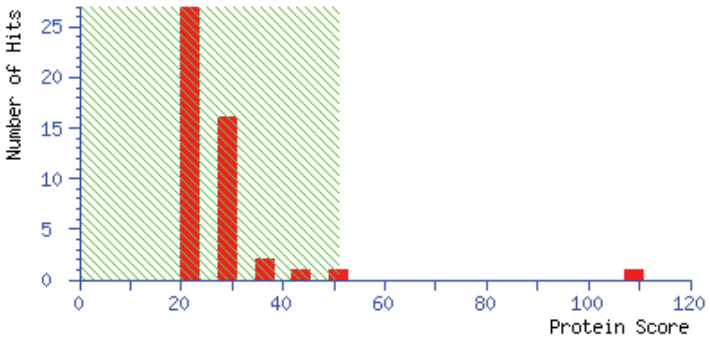

Protein View: YO314_YEAST
Uncharacterized protein YOR314W OS=Saccharomyces cerevisiae (strain ATCC 204508 / S288c) OX=559292 GN=YOR314W PE=4 SV=1

Database:	SwissProt
Score:	52
Expect:	0.052
Monoisotopic mass (Mr):	12743
Calculated pI:	7.66
Taxonomy:	Saccharomyces cerevisiae S288C

Sequence similarity is available as an NCBI BLAST search of YO314_YEAST against nr.

Search parameters
Enzyme:
Trypsin: cuts C-term side of KR unless next residue is P.

Fixed modifications:	Carbamidomethyl (C)
Mass values searched:	79
Mass values matched:	5

Protein sequence coverage: 75%

Matched peptides shown in ***bold red***.

```
  1 MTMIRFCGAR QSAIISNASD AAAGTNKKRI LNPLESLCLN DRIDEHRCKE
 51 VQLSSLRSLL YAMILNRTIG SETGVFSFLL FSFRYFGEER DLFYCFFSVF
101 LLNITYLLD
```

Start	–	End	Observed	Mr(expt)	Mr(calc)	ppm	M	Peptide
6	–	27	2210.0674	2209.0601	2209.0546	2.52	1	R.FCGARQSAIISNASDAAAGTNK.K
11	–	27	1618.8706	1617.8633	1617.7958	41.7	0	R.QSAIISNASDAAAGTNK.K
50	–	67	2106.0534	2105.0461	2105.1666	-57.2	1	K.EVQLSSLRSLLYAMILNR.T
68	–	90	2689.4215	2688.4142	2688.3224	34.1	1	R.TIGSETGVFSFLLFSFRYFGEER.D
85	–	109	3184.8682	3183.8609	3183.5304	104	1	R.YFGEERDLFYCFFSVFLLNITYLLD.-

ID YO314_YEAST Reviewed; 109 AA.
AC Q12506; A0A1S0T0C1;
DT 11-SEP-2007, integrated into UniProtKB/Swiss-Prot.
DT 01-NOV-1996, sequence version 1.
DT 07-APR-2021, entry version 79.
DE RecName: Full=Uncharacterized protein YOR314W;
GN OrderedLocusNames=YOR314W; ORFNames=06123;
OS Saccharomyces cerevisiae (strain ATCC 204508 / S288c) (Baker's yeast).
OC Eukaryota; Fungi; Dikarya; Ascomycota; Saccharomycotina; Saccharomycetes;
OC Saccharomycetales; Saccharomycetaceae; Saccharomyces.
OX NCBI_TaxID=559292;
RN [1]
RP NUCLEOTIDE SEQUENCE [GENOMIC DNA].
RC STRAIN=ATCC 96604 / S288c / FY1679;
RX PubMed=8896266;
RX DOI=10.1002/(sici)1097-0061(199609)12:10b<1021::aid-yea981>3.0.co;2-7;
RA Pearson B.M., Hernando Y., Payne J., Wolf S.S., Kalogeropoulos A.,
RA Schweizer M.;
RT "Sequencing of a 35.71 kb DNA segment on the right arm of yeast chromosome
RT XV reveals regions of similarity to chromosomes I and XIII.";
RL Yeast 12:1021-1031(1996).
RN [2]
RP NUCLEOTIDE SEQUENCE [LARGE SCALE GENOMIC DNA].
RC STRAIN=ATCC 204508 / S288c;
RX PubMed=9169874;
RA Dujon B., Albermann K., Aldea M., Alexandraki D., Ansorge W., Arino J.,
RA Benes V., Bohn C., Bolotin-Fukuhara M., Bordonne R., Boyer J., Camasses A.,

RA Casamayor A., Casas C., Cheret G., Cziepluch C., Daignan-Fornier B.,
RA Dang V.-D., de Haan M., Delius H., Durand P., Fairhead C., Feldmann H.,
RA Gaillon L., Galisson F., Gamo F.-J., Gancedo C., Goffeau A., Goulding S.E.,
RA Grivell L.A., Habbig B., Hand N.J., Hani J., Hattenhorst U., Hebling U.,
RA Hernando Y., Herrero E., Heumann K., Hiesel R., Hilger F., Hofmann B.,
RA Hollenberg C.P., Hughes B., Jauniaux J.-C., Kalogeropoulos A.,
RA Katsoulou C., Kordes E., Lafuente M.J., Landt O., Louis E.J., Maarse A.C.,
RA Madania A., Mannhaupt G., Marck C., Martin R.P., Mewes H.-W., Michaux G.,
RA Paces V., Parle-McDermott A.G., Pearson B.M., Perrin A., Pettersson B.,
RA Poch O., Pohl T.M., Poirey R., Portetelle D., Pujol A., Purnelle B.,
RA Ramezani Rad M., Rechmann S., Schwager C., Schweizer M., Sor F., Sterky F.,
RA Tarassov I.A., Teodoru C., Tettelin H., Thierry A., Tobiasch E.,
RA Tzermia M., Uhlen M., Unseld M., Valens M., Vandenbol M., Vetter I.,
RA Vlcek C., Voet M., Volckaert G., Voss H., Wambutt R., Wedler H.,
RA Wiemann S., Winsor B., Wolfe K.H., Zollner A., Zumstein E., Kleine K.;
RT "The nucleotide sequence of Saccharomyces cerevisiae chromosome XV.";
RL Nature 387:98-102(1997).
RN [3]
RP GENOME REANNOTATION.
RC STRAIN=ATCC 204508 / S288c;
RX PubMed=24374639; DOI=10.1534/g3.113.008995;
RA Engel S.R., Dietrich F.S., Fisk D.G., Binkley G., Balakrishnan R.,
RA Costanzo M.C., Dwight S.S., Hitz B.C., Karra K., Nash R.S., Weng S.,
RA Wong E.D., Lloyd P., Skrzypek M.S., Miyasato S.R., Simison M., Cherry J.M.;
RT "The reference genome sequence of Saccharomyces cerevisiae: Then and now.";
RL G3 (Bethesda) 4:389-398(2014).
RN [4]
RP NUCLEOTIDE SEQUENCE [GENOMIC DNA].
RC STRAIN=ATCC 204508 / S288c;
RX PubMed=17322287; DOI=10.1101/gr.6037607;
RA Hu Y., Rolfs A., Bhullar B., Murthy T.V.S., Zhu C., Berger M.F.,
RA Camargo A.A., Kelley F., McCarron S., Jepson D., Richardson A., Raphael J.,
RA Moreira D., Taycher E., Zuo D., Mohr S., Kane M.F., Williamson J.,
RA Simpson A.J.G., Bulyk M.L., Harlow E., Marsischky G., Kolodner R.D.,
RA LaBaer J.;
RT "Approaching a complete repository of sequence-verified protein-encoding
RT clones for Saccharomyces cerevisiae.";
RL Genome Res. 17:536-543(2007).
CC ----------

DR   EMBL; AY693248; AAT93267.1; -; Genomic_DNA.
DR   EMBL; X90565; CAA62169.1; -; Genomic_DNA.
DR   EMBL; Z75222; CAA99634.1; -; Genomic_DNA.
DR   EMBL; BK006948; DAA80338.1; -; Genomic_DNA.
DR   PIR; S58325; S58325.
DR   SMR; Q12506; -.
DR   DIP; DIP-4454N; -.
DR   IntAct; Q12506; 2.
DR   STRING; 4932.YOR314W; -.
DR   PaxDb; Q12506; -.
DR   PRIDE; Q12506; -.
DR   EnsemblFungi; YOR314W_mRNA; YOR314W; YOR314W.
DR   SGD; S000005841; YOR314W.
DR   HOGENOM; CLU_2186017_0_0_1; -.
DR   PRO; PR:Q12506; -.
DR   Proteomes; UP000002311; Chromosome XV.
DR   RNAct; Q12506; protein.
PE   4: Predicted;
KW   Reference proteome.
FT   CHAIN   1..109
FT   /note="Uncharacterized protein YOR314W"
FT   /id="PRO_0000299735"
SQ   SEQUENCE   109 AA; 12524 MW; C347BF65EEF85121 CRC64;
     MTMIRFCGAR QSAIISNASD AAAGTNKKRI LNPLESLCLN DRIDEHRCKE VQLSSLRSLL
     YAMILNRTIG SETGVFSFLL FSFRYFGEER DLFYCFFSVF LLNITYLLD

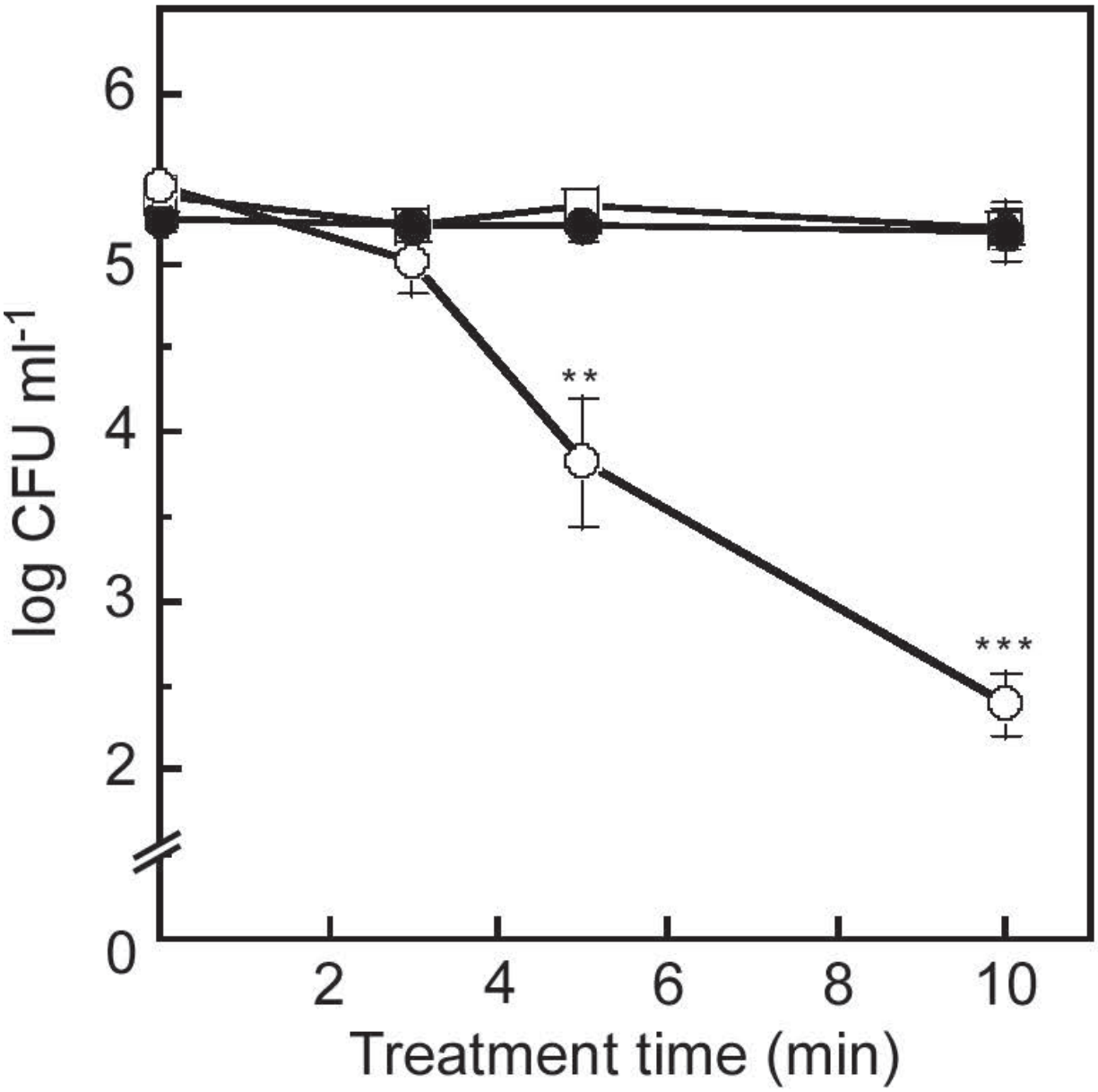

Fig. S1 Time-course analysis of changes in the inactivation of *S. cerevisiae* after each treatment. Initial cells were suspended at a density of 2-3 × 10^5 CFU ml^{-1}. UV-A irradiance was set at 19 mW cm^{-2}. Symbols: UV-A irradiation alone (open squares); 1 mg ml^{-1} FA alone (in the dark, shaded circles); combination of 1 mg ml^{-1} FA and UV-A irradiation (open circles). Data are presented as means ± SD (n=3). Significant differences (**$P < 0.01$ and ***$P < 0.001$; two-tailed, unpaired *t*-test) were determined based on comparison with initial viability.

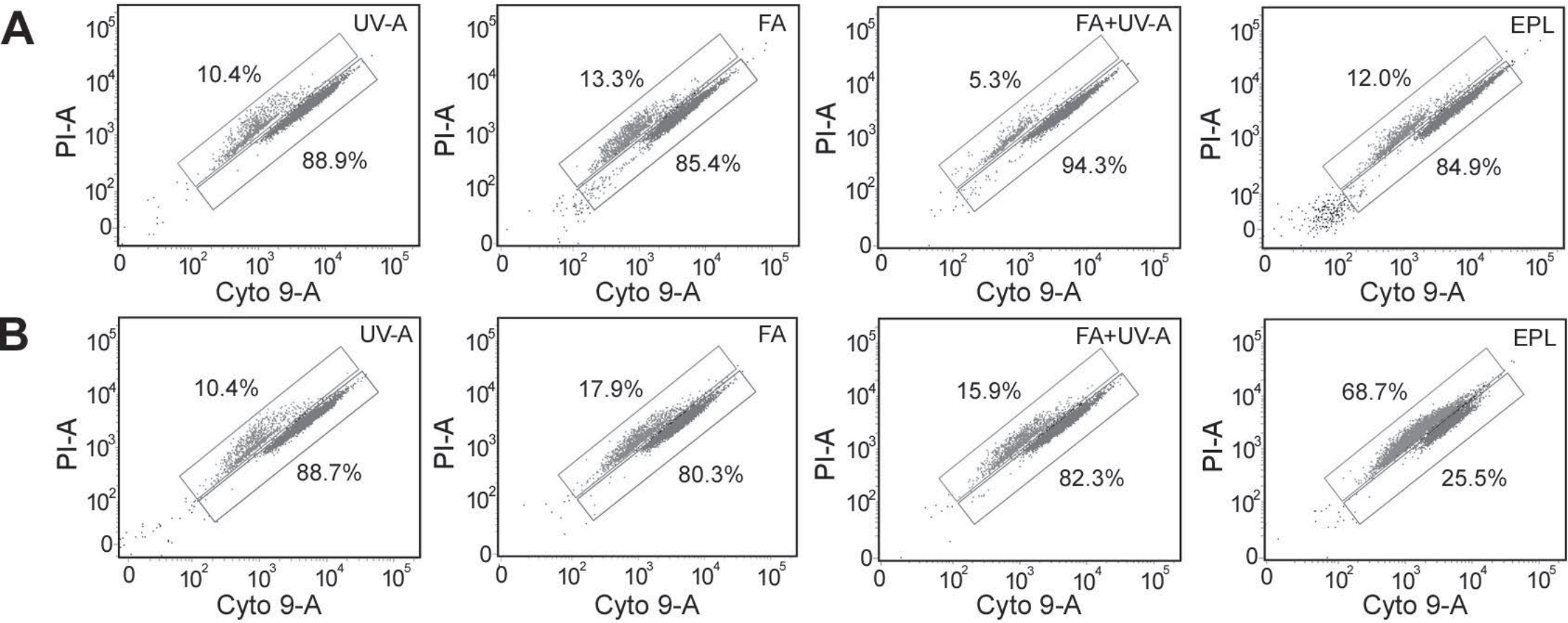

Fig. S2 Dual-parameter dot plots of 10,000 double-stained cells (Cyto 9 and PI) evaluated by flow cytometry after incubation for 0 min (A, upper line) or 5 min (B, lower line). Upper and lower squares indicate PI- (damage or dead) and Cyto 9-stained cells (live), respectively. The numbers near squares in each panel indicate the percentage of live cells and damaged or dead cells among a total of 10,000 cells.

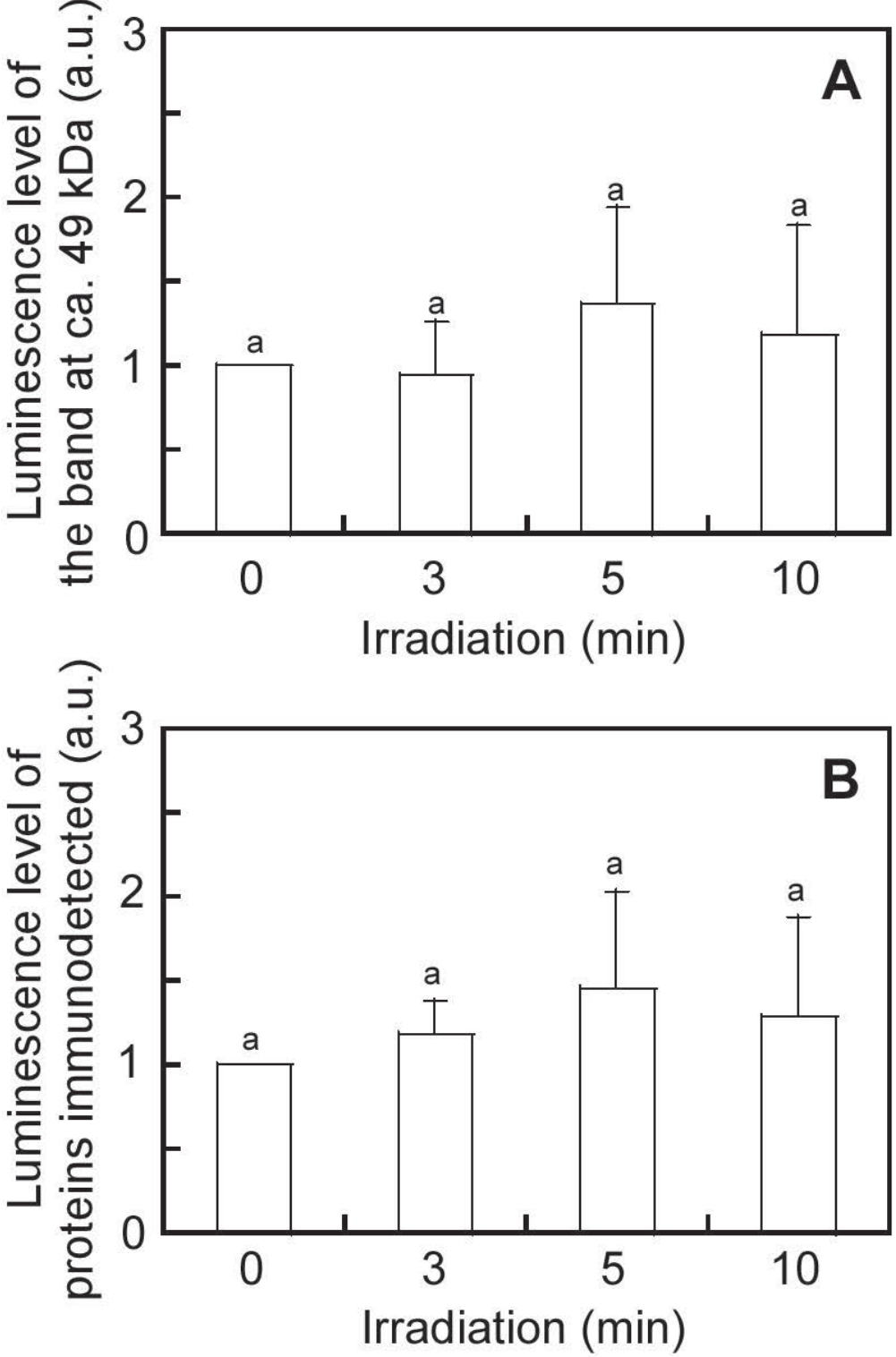

Fig. S3 Oxidative damage of cellular proteins in *S. cerevisiae* treated with UV-A alone at an irradiance of 19 mW cm^{-2}: luminescence levels of the band at ~49 kDa (A) and of proteins (B) immunodetected on Western blots, expressed as arbitrary units (a.u.) of mean luminescence normalized to the signal levels of samples before UV-A irradiation (0 min). Data are presented as the mean ± SD (n=3). Identical letters above the bars indicate no significant differences between groups (one-way ANOVA).

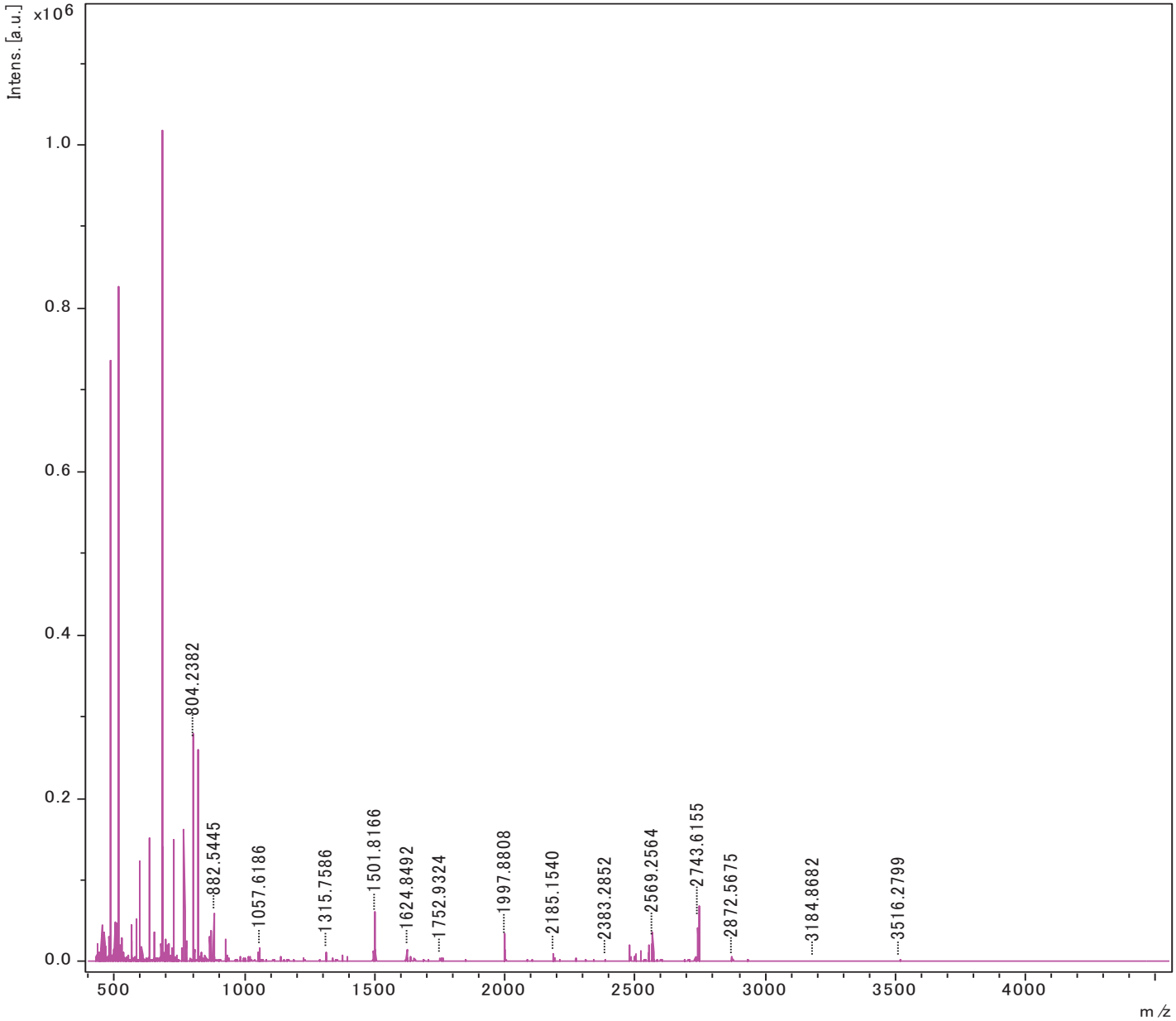

Fig. S4. MALDI-TOF MS spectrum of the peptide produced by in-gel tryptic digestion.

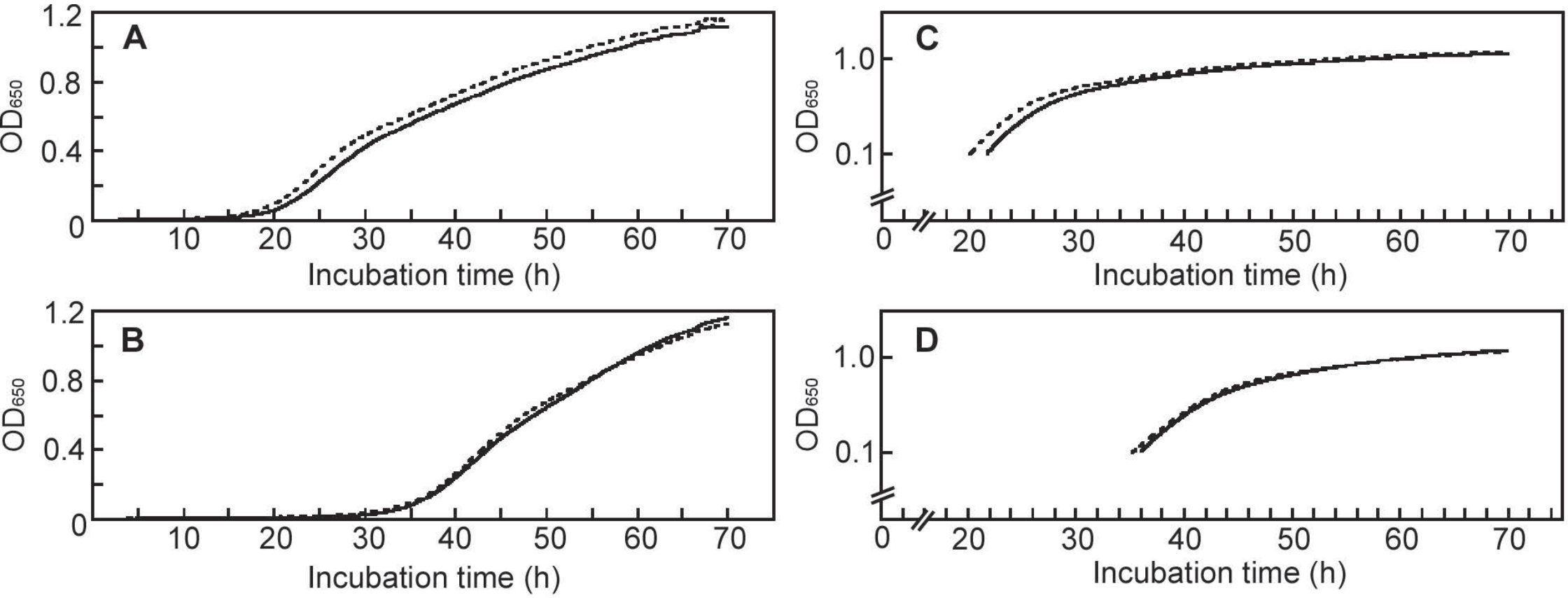

Fig. S5 Effect of treatment with FA and UV-A irradiation on *S. cerevisiae* growth. Growth in each sample was monitored by measuring the optical density at 650 nm (OD_{650}) in panels A and B. As the OD_{650} values were >0.1, the values were plotted on a logarithm scale in panels C and D. Graphs show growth curves for each sample in the absence (A and C) or presence (B and D) of FA. Lines in all figures indicate samples without (solid lines) and with (dotted lines) UV-A irradiation. Values are presented as the mean (n=4).

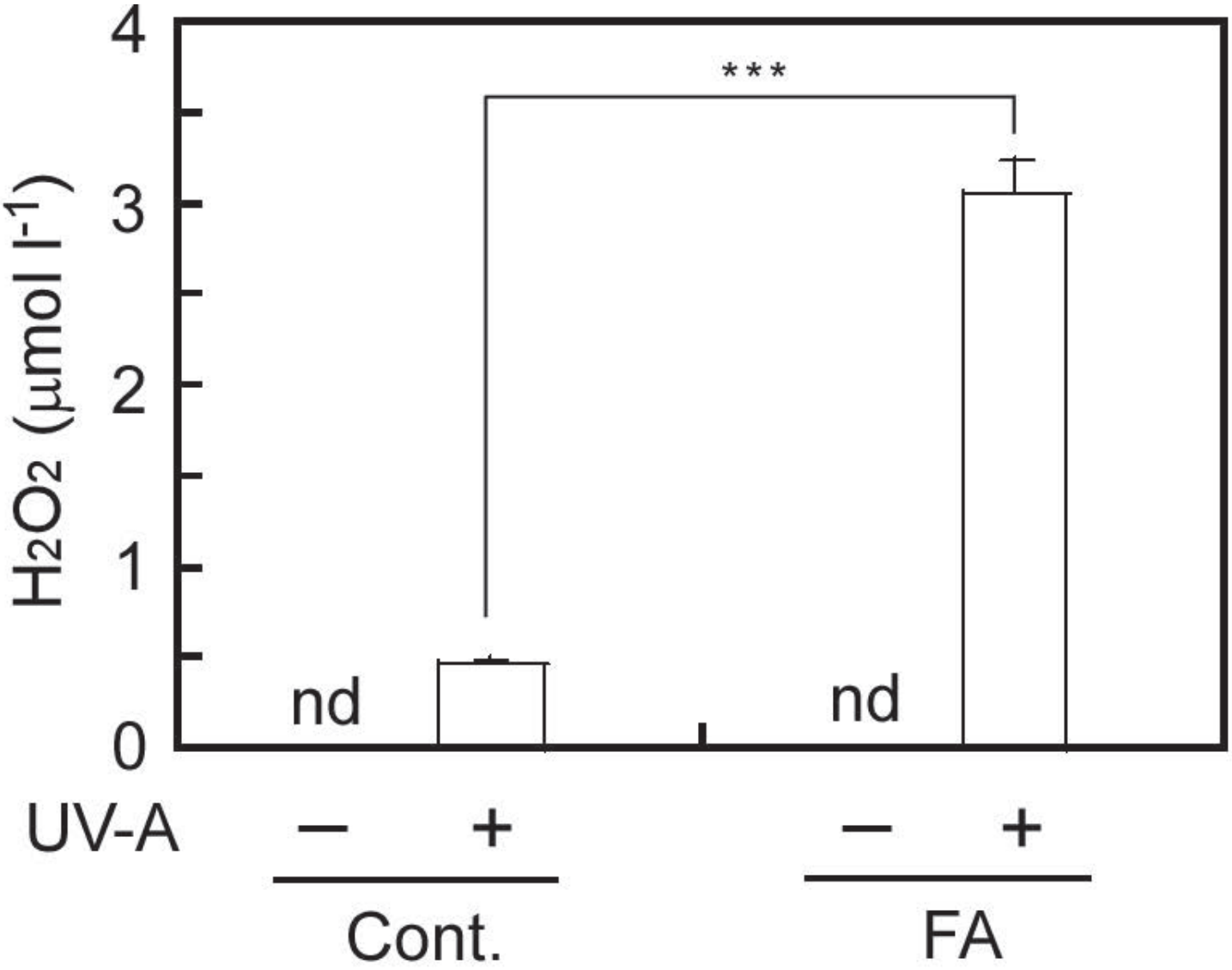

Fig. S6 Concentration of H_2O_2 generated in FA solution with and without UV-A light irradiation. Left and right (open) bars for each treatment indicate H_2O_2 concentration after incubation for 30 min in the dark or UV-A exposure at an irradiance of 4.77 mW cm^{-2}, respectively. Data are presented as means ± SD (n=3). Significant differences (***$P < 0.001$; two-tailed, unpaired t-test). Cont., sample without FA; nd, not detected.

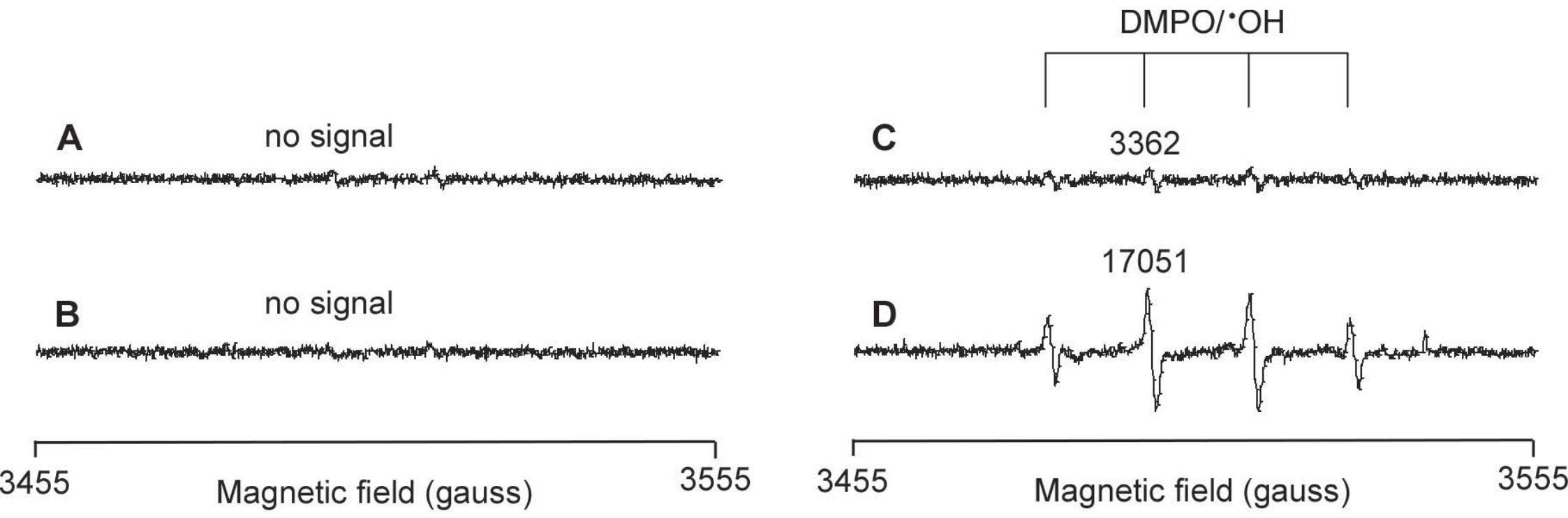

Fig. S7 Formation of 5,5-dimethyl-1-pyrroline-*N*-oxide (DMPO)/•OH adducts in solutions containing phenolic acids before and after irradiation. ESR spectra of mixtures of 4.5 mmol l^{-1} FA and 450 mmol l^{-1} DMPO were recorded before and after irradiation with UV-A light (4.77 mW cm^{-2}) for 3 min. The control sample consisted of 450 mmol l^{-1} DMPO solution prepared with pure water alone. Each figure shows the ESR spectrum for pure water (A and C) and FA (B and D) before (A and B) and after (C and D) irradiation. Values in the figure indicate signal intensity of the second line of the DMPO/•OH adduct graphs (arbitrary units).

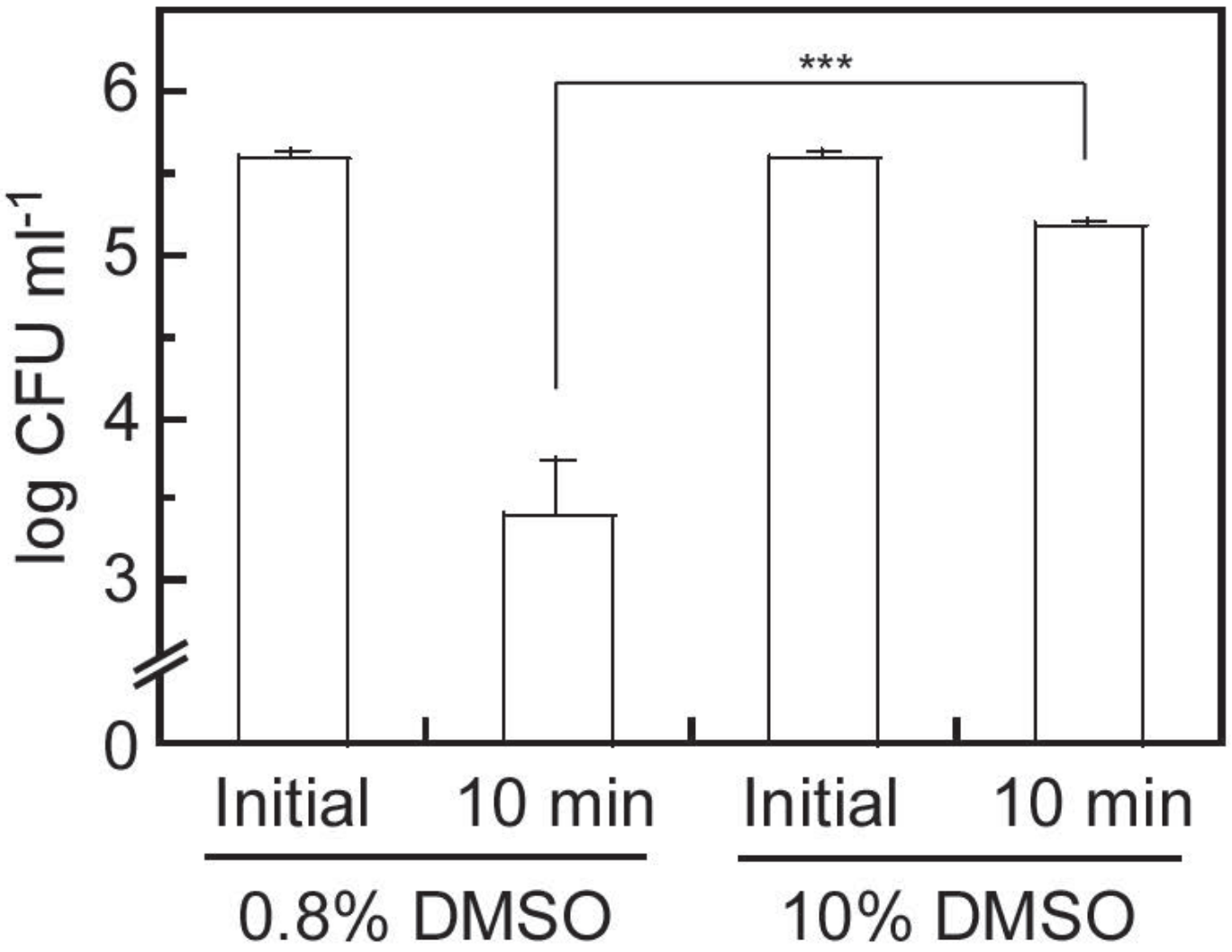

Fig. S8 Effect of DMSO on inactivation of *S. cerevisiae*. Conidia suspensions (initial density, 2-3 $\times$ 10^5 CFU ml^{-1}) were exposed to UV-A irradiation at an irradiance of 19 mW cm^{-2} for 10 min after addition of FA at a concentration of 1 mg ml^{-1} followed by addition of DMSO. Data are presented as the mean $\pm$ SD (n=3). ***$P < 0.001$; two-tailed, unpaired *t*-test.

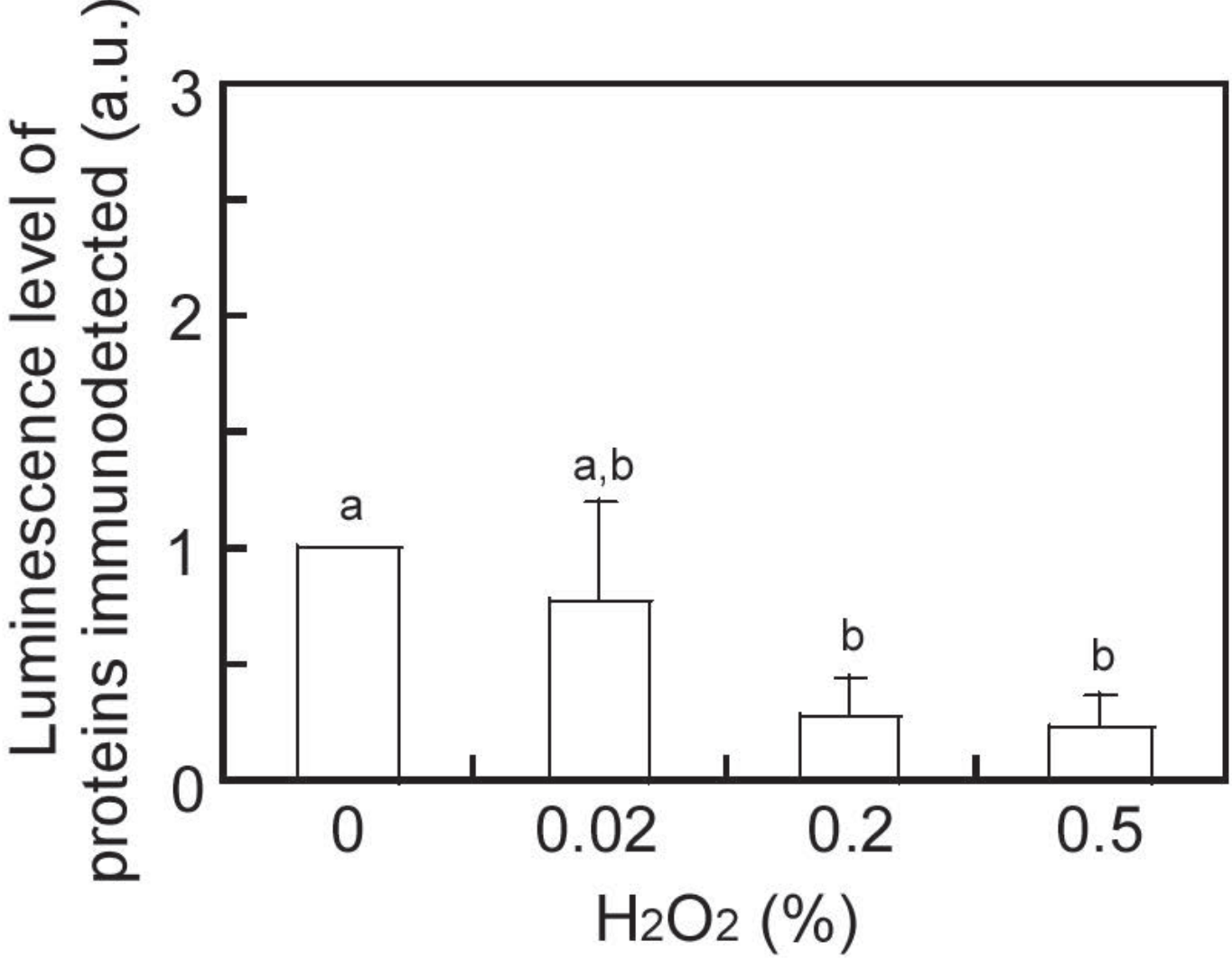

Fig. S9 Oxidative damage of cellular proteins in *S. cerevisiae* (initial density, 2-3 × 10^7 CFU ml^{-1}) treated with H_2O_2 at a concentration of 0.02 to 0.5% for 20 min. Luminescence levels of proteins immunodetected on Western blots, expressed as arbitrary units (a.u.) of mean luminescence normalized to the signal levels of untreated samples. Data are presented as the mean ± SD (n=3). Different letters above the bars denote significant differences between the groups ($P < 0.05$; one-way ANOVA).